Pflugers Arch - Eur J Physiol (2015) 467:267–284
DOI 10.1007/s00424-014-1511-5

Enhanced desensitization followed by unusual resensitization in $GABA_A$ receptors in phospholipase C-related catalytically inactive protein-1/2 double-knockout mice

Hiroki Toyoda · Mitsuru Saito · Hajime Sato · Takuma Tanaka · Takeo Ogawa · Hirofumi Yatani · Tsutomu Kawano · Takashi Kanematsu · Masato Hirata · Youngnam Kang

Received: 22 February 2014 / Revised: 24 March 2014 / Accepted: 27 March 2014 / Published online: 16 April 2014

Abstract Phospholipase C-related catalytically inactive proteins (PRIP-1/2) are previously reported to be involved in the membrane trafficking of $GABA_A$ receptor ($GABA_AR$) and the regulation of intracellular Ca^{2+} stores. $GABA_AR$-mediated currents can be regulated by the intracellular Ca^{2+}. However, in PRIP-1/2 double-knockout (PRIP-DKO) mice, it remains unclear whether the kinetic properties of $GABA_ARs$ are modulated by the altered regulation of intracellular Ca^{2+} stores. Here, we investigated whether $GABA_AR$ currents (I_{GABA}) evoked by GABA puff in layer 3 (L3) pyramidal cells (PCs) of the barrel cortex are altered in PRIP-DKO mice. The deletion of PRIP-1/2 enhanced the desensitization of I_{GABA} but induced a hump-like tail current (tail-I) at the GABA puff offset. I_{GABA} and the hump-like tail-I were suppressed by $GABA_AR$ antagonists. The enhanced desensitization of I_{GABA} and the hump-like tail-I in PRIP-DKO PCs were mediated by increases in the intracellular Ca^{2+} concentration and were largely abolished by a calcineurin inhibitor and ruthenium red. Calcium imaging revealed that Ca^{2+}-induced Ca^{2+} release (CICR) and subsequent store-operated Ca^{2+} entry (SOCE) are more potent in PRIP-DKO PCs than in wild-type PCs. A mathematical model revealed that a slowdown of GABA-unbinding rate and an acceleration of fast desensitization rate by enhancing its GABA concentration dependency are involved in the generation of hump-like tail-Is. These results suggest that in L3 PCs of the barrel cortex in PRIP-DKO mice, the increased calcineurin activity due to the potentiated CICR and SOCE enhances the desensitization of $GABA_ARs$ and slows the GABA-unbinding rate, resulting in their unusual resensitization following removal of GABA.

Keywords PRIP · $GABA_A$ receptor · Desensitization · Calcineurin · Ca^{2+}-induced Ca^{2+} release · Store-operated Ca^{2+} entry

H. Toyoda · M. Saito · H. Sato · T. Ogawa · T. Kawano · Y. Kang (✉)
Department of Neuroscience and Oral Physiology, Osaka University Graduate School of Dentistry, 1-8, Yamadaoka, Suita, Osaka 565-0871, Japan
e-mail: kang@dent.osaka-u.ac.jp

T. Tanaka
Department of Computational Intelligence and Systems Science, Interdisciplinary Graduate School of Science and Engineering, Tokyo Institute of Technology, Yokohama, Kanagawa 226-8502, Japan

H. Yatani
Department of Fixed Prosthodontics, Osaka University Graduate School of Dentistry, 1-8, Yamadaoka, Suita, Osaka 565-0871, Japan

T. Kanematsu
Division of Integrated Medical Science, Department of Dental Pharmacology, Graduate School of Biomedical Sciences, Hiroshima University, Hiroshima 734-8553, Japan

M. Hirata
Laboratory of Molecular and Cellular Biochemistry, Faculty of Dental Science, Kyushu University, Fukuoka 812-8582, Japan

Introduction

The two subtypes of phospholipase C-related but catalytically inactive protein (PRIP-1/2) were first identified as novel inositol 1,4,5-triphosphate (IP_3) binding proteins [21, 22]. Subsequently, they were revealed to be involved in the membrane trafficking of $GABA_A$ receptors ($GABA_ARs$) [23]. In PRIP-1/2 double-knockout (PRIP-DKO) mice, $GABA_A$ currents exhibited a reduced diazepam sensitivity due to a reduced expression of $GABA_ARs$ composed of $\gamma 2$ subunits as a

consequence of the lack of the binding between PRIP-1/2 and $GABA_AR$-associated protein [23], in the hippocampal [30] and the cerebellar granule neurons [31]. On the other hand, PRIP-1 and PRIP-2 were also revealed to be involved in the regulation of intracellular Ca^{2+} stores; IP_3-induced Ca^{2+} release (IICR) was impaired in cultured cortical neurons from PRIP-1 knockout (KO) mice [9] while store-operated Ca^{2+} entry (SOCE) was enhanced in hematopoietic B cells in PRIP-2 KO mice [40]. However, it has not been investigated whether or not the deletion of PRIP-1/2 influences the kinetic properties of $GABA_A$ currents through the altered regulation of intracellular Ca^{2+} stores, in spite of the fact that there is a large body of evidence that $GABA_AR$-mediated currents can be regulated by the intracellular concentration of Ca^{2+} ($[Ca^{2+}]_i$) [12, 39].

Ca^{2+}/calmodulin-dependent protein kinase II enhances $GABA_AR$-mediated currents in spinal dorsal horn neurons [44] and in cerebellar granule neurons [11], while the activation of protein phosphatase 2B (calcineurin) by Ca^{2+} induces a suppression of $GABA_AR$-mediated currents in hippocampal neurons [28] and a slowdown of the rate of GABA unbinding from $GABA_ARs$ [19]. An increase in $[Ca^{2+}]_i$ through the activation of various types of Ca^{2+} channels, including voltage-dependent Ca^{2+} channels and NMDA, IP_3, and ryanodine receptor channels, causes a suppression of $GABA_AR$-mediated currents [5, 15, 32, 42], through the acceleration of desensitization [33]. Considering the altered regulation of intracellular Ca^{2+} stores in PRIP-1 KO and PRIP-2 KO mice [9, 40] together with the finding that layer 2/3 pyramidal cells (PCs) in the rat neocortex express high levels of calcineurin [25, 26], it can be hypothesized that the kinetic properties of $GABA_AR$-mediated currents differ between layer 3 (L3) PCs in wild-type (WT) and PRIP-DKO mice due to putative anomalies in intracellular Ca^{2+} dynamics in PRIP-DKO PCs.

Therefore, in the present study, we investigated the kinetic properties of $GABA_AR$ currents (I_{GABA}) evoked by puff application of GABA and its modulation by manipulation of intracellular Ca^{2+} and Ca^{2+} signaling, in L3 PCs of the barrel cortex in PRIP-DKO mice. Our results suggest that the deletion of PRIP-1/2 results in the enhancement of the desensitization and resensitization of $GABA_ARs$ by the upregulation of Ca^{2+}-dependent activity of calcineurin through the potentiated Ca^{2+}-induced Ca^{2+} release (CICR) and SOCE.

Methods

All experiments were performed in accordance with the guidelines for the care and use of laboratory animals approved by the animal ethics committee of the Osaka University Graduate School of Dentistry.

Slice preparation

PRIP-1/2 double-knockout (PRIP-DKO) mice [30] and WT C57BL/6J mice of both sexes at 15–21 days old were used. PRIP-DKO mice used in this study were back-crossed against the C57BL/6J background [30]. They were anesthetized with ketamine and diethylether, and the brain was quickly removed from the skull and immersed in ice-cold modified artificial cerebrospinal fluid (M-ACSF) composed of 210 sucrose, 2.5 KCl, 2.5 $MgSO_4$, 1.25 NaH_2PO_4, 26 $NaHCO_3$, 0.5 $CaCl_2$, and 50 D-glucose in mM. The rostral part of the brain block including the barrel cortex was cut at 15° tilted caudally from the coronal plane. With a microslicer (Super ZERO-1, Dosaka EM, Kyoto, Japan), sections of 300–350 μm thickness including the whisker barrel were cut parallel to the plane. Slices were incubated at 32 °C for 30 min in 50 % M-ACSF and 50 % normal ACSF (N-ACSF; pH 7.3) composed of 126 NaCl, 3 KCl, 1 $MgSO_4$, 1.25 NaH_2PO_4, 26 $NaHCO_3$, 2 $CaCl_2$, and 10 D-glucose in mM. The slices were then placed in N-ACSF at room temperature (20–24 °C). N-ACSF was continuously gassed with a mixture of 95 % O_2–5 % CO_2.

Whole-cell recording

Using Axopatch 200B (Molecular Devices, Foster City, CA, USA), all whole-cell recordings were made from visually identified PCs in L3 of the barrel cortex under the microscope equipped with Nomarski optics (BX-51WI DIC; Olympus, Tokyo, Japan). The patch pipettes had a DC resistance of 4–5 MΩ when filled with the standard internal solution composed of 130 Cs-gluconate, 10 CsCl, 2 $MgCl_2$, 2 ATP-Na_2, 0.4 GTP-Na_3, 10 HEPES, and 5 EGTA, pH 7.3 adjusted with CsOH in mM. The Cl^- equilibrium potential (E_{Cl}) was calculated to be −57 mV. Voltage-clamp recordings were made at a holding potential of 0 mV (Figs. 1, 2, 4, 5, 6, and 7). In the experiment to investigate the reversal potentials of I_{GABA} and its tail-current (tail-I) (Fig. 3), rundown of I_{GABA} that would affect the current–voltage (I–V) relationship was prevented by substituting 2 mM $MgCl_2$ and 2 mM ATP-Na_2 with 5 mM Mg-ATP and increasing $[EGTA]_i$ from 5 to 10 mM [13]. To maintain E_{Cl} at −57 mV, 130 mM Cs-gluconate was decreased by 4 mM by substituting with equimolar CsCl. The membrane potential values were corrected for the liquid junction potential (10 mV) between the standard internal solution (negative) and the extracellular solution. Using a pressure-pulsed microinjector (4–6 psi; PV830, World Precision Instruments, Sarasota, FL, USA), a puff of 200 μM GABA or 200 μM muscimol for 2 s was repeatedly applied to PCs every minute through a glass pipette, the tip of which was placed 25–50 μm away from their somata. Whole-cell recordings of I_{GABA} were started 10 min after establishing the whole-cell configuration and clamping at 0 mV.

Ca^{2+} imaging using fura-2

To measure $[Ca^{2+}]_i$ changes in L3 PCs of the barrel cortex, slice preparations were incubated in N-ASCF containing 10 μM fura-2 AM (Dojindo Laboratories, Kumamoto, Japan) and 0.01 % Cremophor EL (Sigma-Aldrich, St. Louis, MO, USA) for 60 min at room temperature. Following incubation, the preparations were rinsed with dye-free N-ASCF for 30 min. The recording chamber was mounted on the stage of a fluorescence microscope (BX50WI-FL/DIC; Olympus) equipped with a high-speed cooled digital CCD camera (C6790-80; Hamamatsu Photonics, Hamamatsu, Japan), a high-speed switching light source (C7773; Hamamatsu Photonics), and filter units (U-MWU; DM400/BP330–385/BA420; Olympus). Preparations were observed under a water-immersion objective (LumiPlanFl×40/0.80 or×60/0.90; Olympus) and alternately illuminated at 340 or 380 nm. The fluorescence of 510 nm was captured by the CCD camera at a frame interval of 2 s with an exposure time of 10 ms and stored for offline analysis by an image-processing software (AquaCosmos; Hamamatsu Photonics). Ca^{2+} transients represent changes in the ratio (F_{340}/F_{380}) of the fluorescence at 510 nm excited by 340 nm to that excited by 380 nm as a measure of relative changes in $[Ca^{2+}]_i$. We made the ratiometric measurement only on the visually identified L3 PCs in slice preparations under Nomarski optics (Fig. 8Aa). In the respective slices, clear Ca^{2+} images were simultaneously captured in two to four cells (Fig. 8Ba or Da), which displayed similar Ca^{2+} transients when regions of interest were set on these cells (Fig. 8Bb, Db). A set of parameters were measured in these Ca^{2+} transients, among which a most typical one that had a set of standard parameter values was selected for pooled data analysis to examine statistical differences: *n* stands for the number of these typical cells as well as slices.

Drug application

$GABA_A$R antagonists, 20–50 μM (+)-bicuculline or 100–200 μM picrotoxin, were bath applied. Fenvalerate (a calcineurin inhibitor) and caffeine (a ryanodine receptor agonist) were bath applied at 40 μM and 20 mM, respectively. Ruthenium red (an inhibitor of ryanodine receptor) and calcineurin were added to the internal solution at 100 μM and 0.2 U/ml, respectively. These chemicals except for calcineurin were obtained from Sigma-Aldrich. Calcineurin was obtained from Promega (Madison, WI, USA).

Simulation of I_{GABA}

Simulation of I_{GABA} was performed based on the kinetic model (Fig. 10A [18]). Mathematical calculations were done by using Mathematica 9 (Wolfram Research, Champaign, IL, USA). To simulate the GABA puff responses, the rate constants except for fast desensitization rate (d_2) and GABA-unbinding rate (k_{off}) were set as follows (in s^{-1}): k_{on}= 15 μM^{-1}, r_1=0.35, d_1=6, β_1=200, α_1=1,100, r_2=50, β_2= 2,500, α_2=142, $q=1\times10^{-8}$ μM^{-1}, and P=1. In the present simulation, d_2 was assumed to be dependent on the GABA concentration ([GABA]) as described in "Discussion." The k_{off} values in WT and PRIP-DKO $GABA_A$Rs were set as 90 and 30 s^{-1}, respectively, to simulate the GABA puff responses (Fig. 10C, D). We assumed that the maximum concentration of GABA applied by a puff through a pipette is reduced from 200 to 50 μM on the surface of the recorded cell and that the 2-s GABA puff pulse is attenuated with a time constant of 0.1−0.3 s (Fig. 10C, D, top).

Statistical analysis

Numerical data were expressed as the mean ± SD. The statistical significance was assessed using unpaired (†) or paired (‡) Student's *t* test, ANOVA with Fisher's protected least significant difference post hoc test (*), and single Pearson correlation coefficient ($). $P<0.05$ was considered statistically significant.

Results

Enhancement of I_{GABA} desensitization and subsequent emergence of a hump-like tail-I

First, we analyzed GABA currents (I_{GABA}) evoked in L3 PCs by puff application of GABA to investigate whether and how the deletion of PRIP-1/2 affects kinetic properties of $GABA_A$Rs. The I_{GABA} in PRIP-DKO PCs displayed a more prominent desensitization compared to WT PCs (Fig. 1A, B). Surprisingly, PRIP-DKO PCs displayed a hump-like tail current (tail-I) at the puff offset (Fig. 1B) as if GABA acted as a partial antagonist [1, 2, 36].

The peak amplitude (*a*) and the amplitude at the puff offset (*b*) of the I_{GABA} were measured in 13 WT and 12 PRIP-DKO PCs (Fig. 1A, B), while the peak amplitude of the hump-like tail-I following the puff offset (*c*) was measured in the 12 PRIP-DKO PCs (Fig. 1B). The mean value of $[(a-b)/a]$ as a measure of the desensitization degree (Ds) was significantly ($^{\dagger}P<0.01$) larger in the PRIP-DKO PCs (0.43±0.06) compared to the WT (0.19±0.09) (Fig. 1C). This larger Ds in the PRIP-DKO PCs was accompanied by a longer half-duration, which is the duration at half amplitude of the tail-I at the puff offset (Fig. 1A, B, §). The mean value of the half-duration was significantly ($^{\dagger}P<0.01$) larger in the PRIP-DKO PCs (4.3± 0.5 s) compared to the WT (1.2±0.4 s) (Fig. 1C), due to the presence of the hump-like tail-I. Furthermore, the mean duration of I_{GABA} measured at amplitude of $[(a+b)/2]$, i.e., the mean half-desensitization (half-Ds) time (Fig. 1A, B, #), was

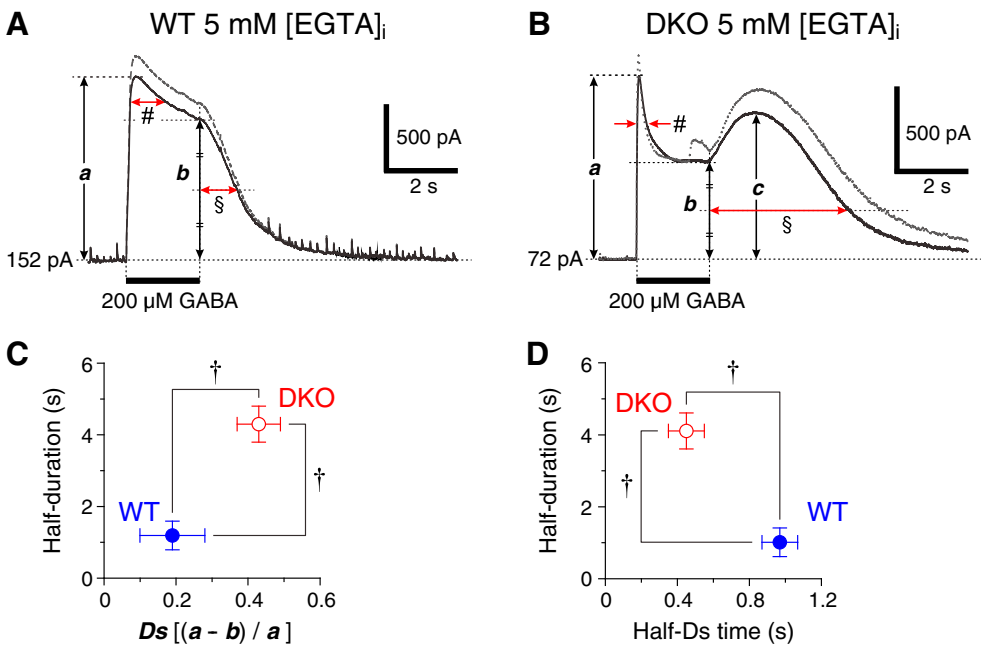

Fig. 1 I_{GABA} evoked by GABA puff applications in WT and PRIP-DKO PCs. **A**, **B** Sample traces of I_{GABA} responses evoked in WT and PRIP-DKO PCs dialyzed with 5 mM EGTA, respectively, at 0 mV by 2-s puff application of GABA with puff-pressures of 4 and 6 psi (*continuous* and *dotted lines*, respectively). *a* The peak amplitude. *b* The amplitude at the offset of puff application. *c* The peak amplitude after the offset of puff application. §The half-duration of the tail-I. #The half-desensitization (half-Ds) time measured at the amplitude of [(*a* + *b*)/2]. **C** The relationship between the desensitization degree [Ds = (*a* – *b*)/*a*] of the I_{GABA} and half-duration of the tail-I (§) induced by a puff with 4 psi. †$P<0.01$. **D** The relationship between the half-Ds time of the I_{GABA} (#) and half-duration of the tail-I (§) induced by a puff with 4 psi. †$P<0.01$

significantly (†$P<0.01$) shorter in the PRIP-DKO PCs (0.45 ±0.10 s) compared to the WT (0.97±0.10 s) (Fig. 1D). Similarly, this shorter half-Ds time in the PRIP-DKO PCs was accompanied by the longer half-duration of the tail-I. These results clearly indicate that the desensitization of I_{GABA} was stronger in PRIP-DKO PCs than in WT PCs and suggest that in PRIP-DKO PCs the prominent hump-like tail-I is induced as a rebound response from the stronger desensitization of I_{GABA}, consistent with the previously proposed idea that the desensitization of $GABA_A$Rs is mechanistically related to the deactivation [18]. The hump-like tail-I amplitude ($c - b$) was normalized to the peak amplitude (a) of I_{GABA} to obtain [($c - b$)/a] as a measure of resensitization degree (Rs). Rs was 0.18±0.05 in the PRIP-DKO PCs (Fig. 1B).

Effects of $GABA_A$R antagonists on I_{GABA} and hump-like tail-Is in PRIP-DKO PCs

Next, to investigate whether or not the hump-like tail-I as well as I_{GABA} observed in PRIP-DKO PCs is carried through $GABA_A$R-coupled Cl^- channels, we examined the effects of picrotoxin on I_{GABA} and its tail-Is evoked in PRIP-DKO PCs dialyzed with 5 mM EGTA (n=6). Following bath application of 200 μM picrotoxin, the I_{GABA} and hump-like tail-Is were progressively suppressed (Fig. 2Aa), and the small current that remained 11 min after application of picrotoxin was completely abolished by an addition of 20 μM bicuculline in the extracellular solution containing picrotoxin (bottom trace). These observations clearly indicate that the I_{GABA} is generated by the activity of $GABA_A$Rs. It is noteworthy that at 1–2 min after application of picrotoxin, the peak I_{GABA} was largely suppressed in parallel with its tail-I (Fig. 2A). Indeed, the analysis of the progress of I_{GABA} blockade by picrotoxin revealed a close relationship between the peak I_{GABA} and tail-I. Changes in the amplitudes of I_{GABA} following application of picrotoxin (Fig. 2Aa) were measured at the three time points: the peak time of the control I_{GABA} (triangle), the offset of puff application (square), and the time point after the half of the half-duration of the control tail-I from the puff offset (circle), namely 1/2 half-duration, and these amplitudes were normalized to their controls. As shown in Fig. 2Ab, the amplitudes at the peak time and at the 1/2 half-duration were more markedly suppressed after application of picrotoxin, compared with that at the puff offset. This differential blockade by picrotoxin between the amplitudes of I_{GABA} at its peak and the puff offset was consistent with the effects of picrotoxin on $GABA_A$ current in frog sensory neurons [16]. At the end of GABA puff, there are many $GABA_A$R channels in the desensitized state, to which picrotoxin preferentially binds [35, 37]. Then, the probability of blockade of activated $GABA_A$R channels by picrotoxin would become smaller as the desensitization progresses, consequently causing less prominent blockade at

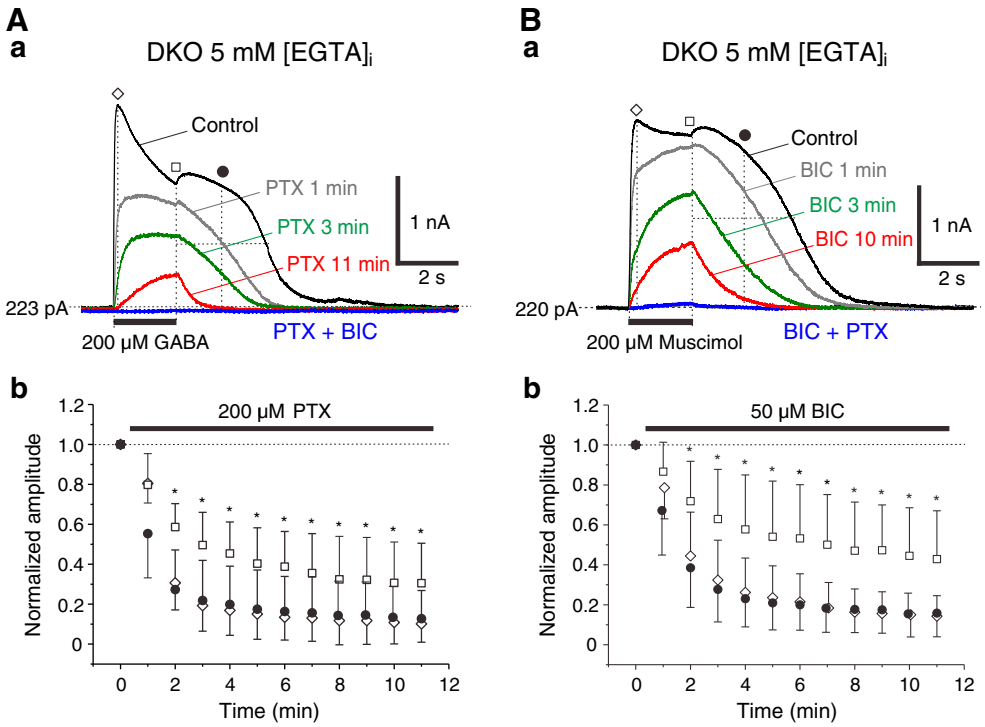

Fig. 2 Effects of $GABA_AR$ antagonists on I_{GABA} and I_{Mus} in PRIP-DKO PCs. **A***a* Superimposed sample traces of I_{GABA} evoked by 200 μM GABA puff application obtained before and 1, 3, and 11 min after application of 200 μM picrotoxin (*PTX*) and 5 min after subsequent co-application of PTX and 20 μM bicuculline (*BIC*) in PRIP-DKO PCs dialyzed with 5 mM EGTA. **B***a* Superimposed sample traces of muscimol-induced currents (I_{Mus}) evoked by 200 μM muscimol puff application obtained before and 1, 3, and 10 min after application of 50 μM BIC and 5 min after subsequent co-application of BIC and 100 μM PTX in PRIP-DKO PCs dialyzed with 5 mM EGTA. The mean Ds, half-Ds time, Rs, and half-duration of the tail-I of I_{Mus} were 0.21±0.11, 0.90±0.18 s, 0.08±0.03, and 4.84±0.98 s, respectively (n=5). **A***b*, **B***b* Plotting of the normalized amplitudes of I_{GABA} (**A***b*) or I_{Mus} (**B***b*) following application of PTX or BIC, which were measured at the three time points: the peak time of the control I_{GABA} (*diamond*), the offset of puff application (*square*), and the time point after the half of the half-duration of the control tail-I from the puff offset (*circle*). The amplitudes at the peak time of I_{GABA} and I_{Mus} and at the 1/2 half-duration were significantly smaller (*P<0.05 and *P<0.05, respectively) than those at the puff offset at the latest 2 min after application of PTX and BIC, respectively

the puff offset compared to the peak I_{GABA}. Because picrotoxin markedly suppressed the tail-I in parallel with the peak I_{GABA} that undergoes desensitization, the desensitized $GABA_AR$ channels are likely to be resensitized at the offset of GABA puff. These results would indicate that the hump-like tail-I, as well as I_{GABA}, is generated by the activity of $GABA_AR$ channels.

To further confirm the sole involvement of $GABA_ARs$ in generating I_{GABA} and its tail-I, muscimol, a $GABA_AR$ agonist, was puff-applied in PRIP-DKO PCs dialyzed with 5 mM EGTA. Similar to the responses to GABA puff, a hump-like tail-I was induced at the offset of 200 μM muscimol puff application (Fig. 2Ba). The mean Ds in muscimol-induced currents (I_{Mus}) was significantly smaller ($^{\dagger}P$<0.01, n=5) than that in I_{GABA} (Fig. 1C), and the mean half-Ds time in I_{Mus} was significantly longer ($^{\dagger}P$<0.01) compared to the I_{GABA} (Fig. 1D). Furthermore, the mean Rs in I_{Mus} was significantly smaller ($^{\dagger}P$<0.01) compared to the I_{GABA}, although there was no significant difference ($^{\dagger}P$>0.2, n=5) in the mean half-duration of the tail-I between I_{Mus} and I_{GABA}. Thus, I_{Mus} displayed less apparent desensitization and resensitization compared to I_{GABA}, in spite of a similar desensitization rate between I_{Mus} and I_{GABA} [20]. This may be because both the deactivation rate of $GABA_ARs$ and the agonist unbinding rate become slower when $GABA_ARs$ are activated by muscimol, compared to the case with GABA [20]. Indeed, our simulation study revealed that simulated I_{GABA} displayed less desensitization and resensitization after decreasing the deactivation rates (α_1 and α_2) and unbinding rate (k_{off}) (figure not shown).

We then examined the effects of bicuculline on the I_{Mus} and its tail-Is. Following bath application of 50 μM bicuculline, the I_{Mus} and its tail-I were progressively suppressed after application of bicuculline (Fig. 2Ba), and the small current remained 10 min after application of bicuculline was completely abolished by an addition of 100 μM picrotoxin in the extracellular solution containing bicuculline (bottom trace). Similar to the case with the blockade of I_{GABA} by picrotoxin, the analysis of the progress of I_{Mus} suppression by bicuculline revealed a close relationship between the desensitization and resensitization of I_{Mus} (Fig. 2Bb). Taken together, these results strongly suggest the hump-like tail-Is as well as I_{GABA} are mediated by the activity of $GABA_AR$ channels.

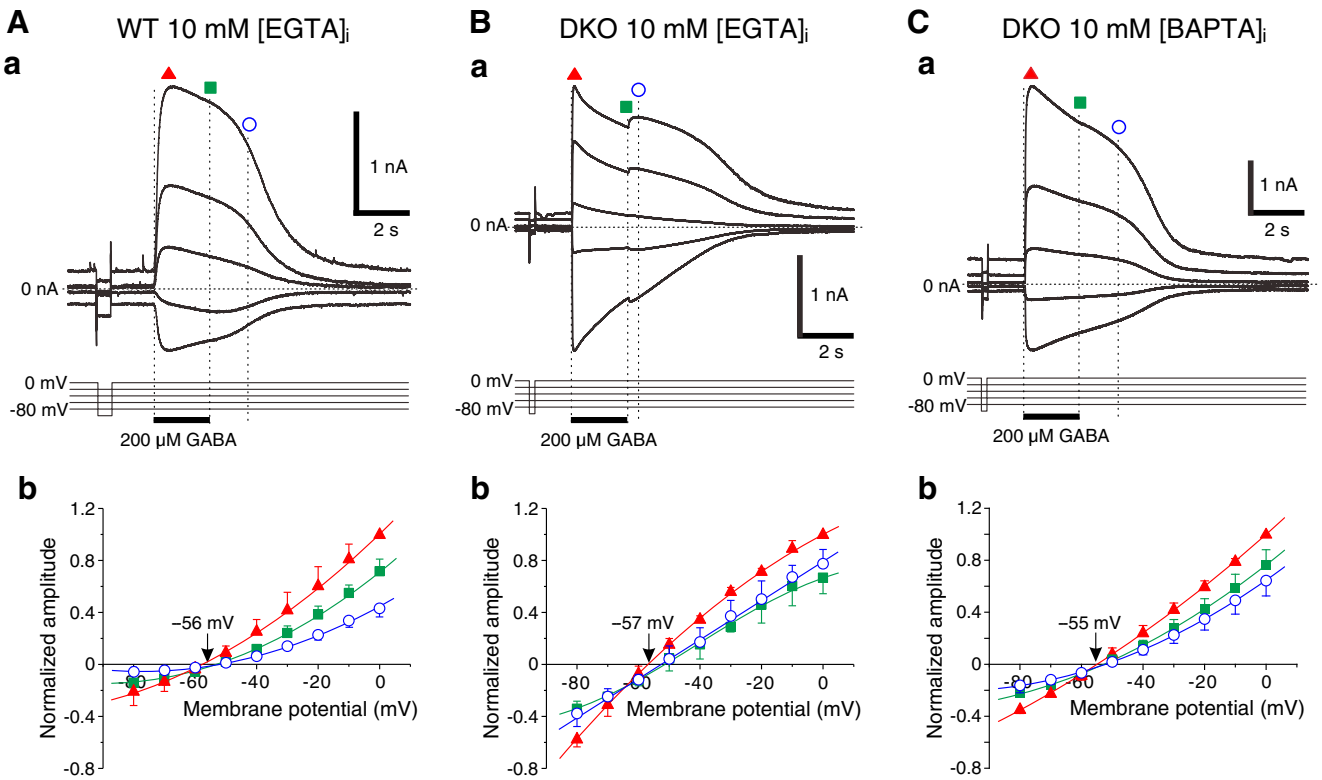

Fig. 3 I–V relationships of I_{GABA} in WT and PRIP-DKO PCs. **A***a*, **B***a*, **C***a* Sample traces of I_{GABA} induced by puff applications of GABA at different holding potentials in WT and PRIP-DKO PCs dialyzed with 10 mM EGTA (**A***a* and **B***a*, respectively) and in PRIP-DKO PCs dialyzed with 10 mM BAPTA (**C***a*). **A***b*, **B***b*, **C***b* The mean I–V relationships for I_{GABA} evoked in WT and PRIP-DKO PCs dialyzed with 10 mM EGTA (**A***b* and **B***b*, respectively) and in PRIP-DKO PCs dialyzed with 10 mM BAPTA (**C***b*), measured at three time points: the time point of peak I_{GABA} (*triangles*), the offset of puff application (*squares*), and 1.5 s after the offset of puff application (*circles*, **A***b* and **C***b*) or the time point of peak tail-Is (*circles*, **B***b*). Respective amplitudes of I_{GABA} measured at the three time points were normalized to the peak amplitude of I_{GABA} evoked at 0 mV. There were no significant (**P*>0.06, *n*=5) differences in the mean reversal potentials between the I_{GABA} at the three time points in the PRIP-DKO PCs dialyzed with BAPTA (−55±3, −53±1, and −52±2 mV). The residual amplitudes of outward I_{GABA} evoked at holding potentials between −50 and 0 mV were calculated from the linear regression of the peak amplitudes of the inward I_{GABA} evoked at holding potentials between −80 and −60 mV. The correlation coefficients of the residuals of the amplitudes of I_{GABA} recorded with 10 mM EGTA and BAPTA were −0.97±0.01 and 0.98±0.02, respectively, which indicate significant inward and outward rectification, respectively ($^{\$}P$<0.01 and $^{\$}P$<0.01).

Reversal potentials of I_{GABA} and hump-like tail-Is

It is still possible that the generation of the hump-like tail-I is secondary to $GABA_AR$-mediated I_{GABA}. To rule out this possibility and to confirm that both the hump-like tail-Is and I_{GABA} are carried by Cl^- through $GABA_AR$ channels, the reversal potentials of I_{GABA} and its tail-Is were examined. The I–V relationships obtained in WT and PRIP-DKO PCs dialyzed with 10 mM EGTA were examined at three time points: the time point of peak I_{GABA} (Fig. 3Aa, Ba, triangles), the offset of puff application (Fig. 3Aa, Ba, squares), and 1.5 s after the offset of puff application (Fig. 3Aa, circle) or the time point of peak tail-Is (Fig. 3Ba, 1.2±0.5 s after the puff offset, *n*=5; circle). In WT PCs dialyzed with 10 mM EGTA (*n*=5), all of the I–V relationships measured at the three time points invariably displayed an outward rectification (Fig. 3Ab), consistent with the previous report [3]. The reversal potentials of the I_{GABA} measured at the three time points were almost the same as the Cl^- equilibrium potential (E_{Cl}=−57 mV). In contrast, in PRIP-DKO PCs dialyzed with 10 mM EGTA (*n*=5), the I–V relationship measured at the time point of the peak amplitude (Fig. 3Ba, triangle) displayed a significant inward rectification ($^{\$}P$<0.01, *n*=5; Fig. 3Bb, triangles), while those measured at the puff offset and the time point of peak tail-Is (Fig. 3Ba, square and circle, respectively) displayed a slight inward and no apparent rectification, respectively (Fig. 3Bb, squares and circles, respectively). There were no significant (WT, **P*>0.1; PRIP-DKO, **P*>0.4) differences in the mean reversal potentials between the I_{GABA} at the three time points in the WT (−56±1, −53±3, and −54±4 mV, *n*=5) and PRIP-DKO PCs (−57±2, −54±4, and −53±5 mV, *n*=5). All these reversal potentials were nearly equal to the E_{Cl}, indicating that the hump-like tail-Is as well as I_{GABA} are carried by Cl^- through $GABA_AR$ channels. This result suggests that the rebound hump-like tail-I is mediated by an unusual reopening of $GABA_ARs$ induced at the offset of GABA puff application.

In PRIP-DKO PCs dialyzed with 10 mM BAPTA, the I_{GABA} recorded at 0 mV exhibited less prominent desensitization and

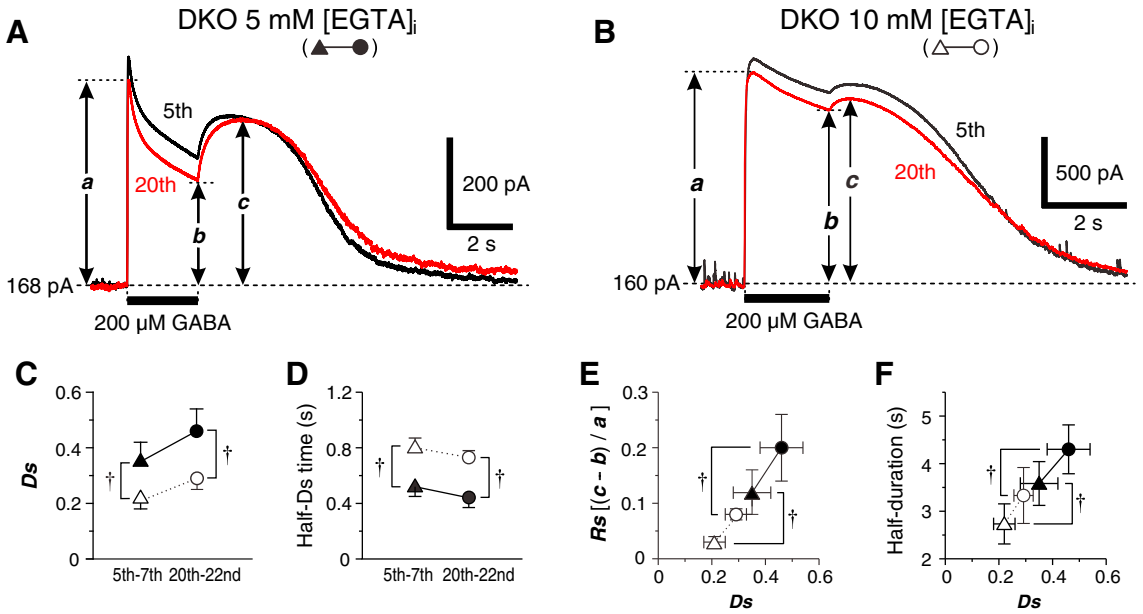

Fig. 4 Effects of EGTA on the desensitization and resensitization of I_{GABA} in PRIP-DKO PCs. **A**, **B** Sample traces of the fifth and the 20th I_{GABA} evoked in PRIP-DKO PCs dialyzed with 5 mM EGTA (**A**) and dialyzed with 10 mM EGTA (**B**) by repeated puff application of GABA every minute. **C** The mean Ds in the fifth–seventh (*triangles*) and the 20th–22nd averaged I_{GABA} (*circles*) evoked in the PRIP-DKO PCs dialyzed with 5 mM EGTA (*filled symbols*: 0.35±0.07 and 0.46±0.08, respectively, n=6) and in those dialyzed with 10 mM EGTA (*open symbols*: 0.22±0.04 and 0.29±0.04, respectively, n=5). $^{\dagger}P<0.01$. **D** The mean half-Ds time in the fifth–seventh and the 20th–22nd averaged I_{GABA} evoked in the PRIP-DKO PCs dialyzed with 5 mM EGTA (0.52± 0.07 and 0.44±0.07 s, respectively, n=6) and in those dialyzed with 10 mM EGTA (0.80±0.07 and 0.73±0.05 s, respectively, n=5). $^{\dagger}P<0.01$. **E** The relationship between the Ds and resensitization degree [Rs=(c − b)/a] in the fifth–seventh (*triangles*) and the 20th–22nd averaged I_{GABA} (*circles*) evoked in the PRIP-DKO PCs dialyzed with 5 mM EGTA (Rs: 0.12±0.04 and 0.20±0.06, respectively, n=6) and in those evoked in the PRIP-DKO PCs dialyzed with 10 mM EGTA (Rs: 0.03± 0.01 and 0.08±0.01, respectively, n=5). $^{\dagger}P<0.01$. **F** The relationship between the Ds and half-duration of the tail-I in the fifth–seventh and the 20th–22nd averaged I_{GABA} evoked in the PRIP-DKO PCs dialyzed with 5 mM EGTA (half-duration: 3.58±0.46 and 4.30±0.51 s, respectively, n=6) and in those evoked in the PRIP-DKO PCs dialyzed with 10 mM EGTA (half-duration: 2.73±0.42 and 3.37±0.63 s, respectively, n=5). $^{\dagger}P<0.02$

was followed by little hump-like tail-Is (Fig. 3Ca), compared to those dialyzed with 10 mM EGTA (Fig. 3Ba). Indeed, the Ds (0.19±0.05) and half-Ds time (0.94±0.04 s) in PRIP-DKO PCs dialyzed with 10 mM BAPTA (n=5) were significantly ($^{\dagger}P<0.05$) smaller and longer than the Ds (0.28±0.04) and half-Ds time (0.70±0.10 s) in those dialyzed with 10 mM EGTA (n=5), respectively. The I–V relationships at the three time points in the I_{GABA} recorded with 10 mM BAPTA were outwardly rectifying with the reversal potentials close to the E_{Cl} (Fig. 3Cb). In contrast to the I_{GABA} recorded with 10 mM EGTA, the I–V relationship of the peak I_{GABA} recorded with 10 mM BAPTA displayed a significant outward rectification ($^{\$}P<0.01$, n=5). Then, the inward rectification of the I–V relationship of the peak I_{GABA} in PRIP-DKO PCs recorded with 10 mM EGTA is likely to be mediated by Ca^{2+}-dependent desensitization of I_{GABA} that became more pronounced as the holding potential was more depolarized to activate voltage-dependent Ca^{2+} channels. The difference in the rectification between PRIP-DKO PCs recorded with 10 mM EGTA and BAPTA appeared to be consistent with the difference in the desensitization between those. Furthermore, both the desensitization and reactivation of I_{GABA} appeared to be dependent on $[Ca^{2+}]_i$. Thus, the reactivation or resensitization of I_{GABA} appeared to be correlated with the desensitization degree of I_{GABA} in a Ca^{2+}-dependent manner.

Enhancement of the desensitization and resensitization of I_{GABA} in PRIP-DKO PCs by increases in $[Ca^{2+}]_i$

Because the desensitization of $GABA_AR$ is well-known to be accelerated by increases in $[Ca^{2+}]_i$ [33], the effects of $[Ca^{2+}]_i$ on the desensitization of I_{GABA} and the generation of tail-I in PRIP-DKO PCs were examined using two different pipette solutions that contained 5 or 10 mM EGTA. The I_{GABA} evoked at 0 mV in PRIP-DKO PCs dialyzed with 5 mM EGTA displayed a more prominent desensitization and was followed by a more prominent hump-like tail-I compared to those dialyzed with 10 mM EGTA (Fig. 4A, B). With the repetition of puff applications of GABA for 2 s every minute, the desensitization of I_{GABA} evoked in PCs dialyzed with 5 mM EGTA appeared to progress and the hump-like tail-I appeared to be enhanced, as shown in the superimposed traces of the fifth and the 20th I_{GABA} (Fig. 4A). Such changes appeared to be less clear in PCs dialyzed with 10 mM EGTA (Fig. 4B). The mean Ds in the respective averaged responses of the fifth–seventh and the 20th–22nd I_{GABA} were

significantly and consistently larger ($^{\dagger}P<0.01$) in the PCs dialyzed with 5 mM EGTA ($n=6$) compared to those dialyzed with 10 mM EGTA ($n=5$) (Fig. 4C). Furthermore, the mean half-Ds time in the fifth–seventh and that in the 20th–22nd averaged I_{GABA} was also significantly and consistently shorter ($^{\dagger}P<0.01$) in the PCs dialyzed with 5 mM EGTA than in those dialyzed with 10 mM EGTA (Fig. 4D). These results clearly indicate that the desensitization of I_{GABA} observed in PRIP-DKO PCs was accelerated depending on free $[Ca^{2+}]_i$.

Because the probability of reopening or resensitization would increase as the number of desensitized $GABA_AR$ channels increases [18], the relationship between the degrees of desensitization and resensitization was examined by plotting the Rs (= $(c - b)/a$) against Ds. As seen in the scattergram (Fig. 4E), both the mean Ds and Rs in the fifth–seventh and the 20th–22nd averaged I_{GABA} in the PCs dialyzed with 5 mM EGTA (filled triangle and circle) were significantly and consistently larger ($^{\dagger}P<0.01$) than in those in the PCs dialyzed with 10 mM EGTA (open triangle and circle), respectively. Thus, the larger Rs invariably accompanied the larger Ds observed in the PCs dialyzed with EGTA at the lower concentration, regardless of the trials of GABA puff applications. Similarly, the significantly larger ($^{\dagger}P<0.02$) mean half-duration of the hump-like tail-I invariably accompanied the larger Ds observed in the PCs dialyzed with EGTA at the lower concentration, regardless of the trials of GABA puff applications (Fig. 4F).

Taken together, these results clearly indicate that both the desensitization and resensitization of I_{GABA} in PRIP-DKO PCs are dependent on $[Ca^{2+}]_i$. This suggests that $[Ca^{2+}]_i$ may be higher in PRIP-DKO PCs than in WT PCs at a holding potential of 0 mV. Both the Ds and Rs increased after repeated application of GABA over 22 trials, probably due to an increase in $[Ca^{2+}]_i$ during a long recording at 0 mV. This phenomenon was used as a control for the experiments described below.

Effects of changes in $[Ca^{2+}]_o$ on I_{GABA} in PRIP-DKO PCs

We next investigated the possible Ca^{2+}-dependent relationship between the desensitization and resensitization of I_{GABA} in PRIP-DKO PCs, by examining how the I_{GABA} and its tail-I evoked at 0 mV in PRIP-DKO PCs dialyzed with 5 mM EGTA are altered following an increase in $[Ca^{2+}]_o$ from 0.5 to 2 mM. As the WT PCs never displayed a hump-like tail-I regardless of EGTA concentration (figure not shown), only PRIP-DKO mice were examined in this experiment.

Whole-cell recordings were made from PRIP-DKO PCs in such slices that were pre-incubated for 30 min in the extracellular solution containing 0.5 mM Ca^{2+}. I_{GABA} was repeatedly evoked by seven trials of GABA puff application every minute in 0.5 mM $[Ca^{2+}]_o$ and also repeatedly evoked by over 15 trials of GABA puff application every minute after $[Ca^{2+}]_o$ was increased from 0.5 to 2 mM. The averaged I_{GABA} evoked by the fifth–seventh GABA puffs at 0 mV in 0.5 mM $[Ca^{2+}]_o$ displayed much less desensitization and was followed by a very small hump-like tail-I (Fig. 5Aa), in contrast to the fifth–seventh averaged I_{GABA} evoked in 2 mM $[Ca^{2+}]_o$ in the different sample groups (Fig. 4A). However, after $[Ca^{2+}]_o$ was increased from 0.5 to 2 mM, the averaged I_{GABA} evoked by the 13th–15th GABA puffs which correspond to the 20th–22nd ones after starting the whole-cell recording displayed a prominent desensitization and was followed by a prominent hump-like tail-I at the offset of the GABA puff (Fig. 5Aa), similar to the fifth–seventh averaged I_{GABA} evoked at 2 mM $[Ca^{2+}]_o$ in the different sample groups (Fig. 4A).

As illustrated in Fig. 5Ab, Ac), the mean values of the Ds and half-Ds time in the averaged I_{GABA} evoked by the fifth–seventh GABA puffs in 0.5 mM $[Ca^{2+}]_o$ (open triangles: 0.08±0.03 and 0.96±0.12 s, respectively) were significantly ($^{\dagger}P<0.01$ and $^{\dagger}P<0.01$, respectively, $n=7$) different from those in the fifth–seventh averaged I_{GABA} in 2 mM $[Ca^{2+}]_o$ shown in Fig. 4C, D (gray triangles). However, when compared between these two averaged I_{GABA} evoked before and after $[Ca^{2+}]_o$ was increased from 0.5 to 2 mM, the mean Ds and half-Ds time were significantly ($n=7$) increased to 0.35±0.10 ($^{\ddagger}P<0.01$) and decreased to 0.59±0.16 s ($^{\ddagger}P<0.01$), respectively (Fig. 5Ab, Ac), compare open triangles and circles). Consequently, the former and latter parameters in the averaged I_{GABA} evoked in 2 mM $[Ca^{2+}]_o$ corresponding to the 20th–22nd averaged I_{GABA} became similar ($^{\dagger}P>0.9$ and $^{\dagger}P>0.6$, respectively) to those in the fifth–seventh averaged I_{GABA} in 2 mM $[Ca^{2+}]_o$ (Fig. 5Ab, Ac), compare open circles and gray triangles). These results indicate that the desensitization of I_{GABA} observed in PRIP-DKO PCs at 0.5 mM $[Ca^{2+}]_o$ was weak but became prominent due to a $[Ca^{2+}]_o$ increase to 2 mM, rather than due to the repetition of GABA puff application.

As seen in the scattergrams (Fig. 5Ad, Ae), the mean values of the Rs and half-duration in the averaged I_{GABA} evoked by the fifth–seventh GABA puffs in 0.5 mM $[Ca^{2+}]_o$ (open triangles: 0.04±0.02 and 2.74±0.62 s, respectively) were significantly ($^{\dagger}P<0.01$ and $^{\dagger}P<0.03$, respectively, $n=7$) smaller than those in the fifth–seventh averaged I_{GABA} in 2 mM $[Ca^{2+}]_o$ (gray triangles). However, when compared between these two averaged I_{GABA} evoked before and after $[Ca^{2+}]_o$ was increased from 0.5 to 2 mM, the mean Rs and half-duration were significantly ($n=7$) increased to 0.11±0.04 ($^{\ddagger}P<0.01$) and 3.72±0.57 s ($^{\ddagger}P<0.01$), respectively (Fig. 5Ad, A e), compare open triangles and circles). Consequently, the former and latter parameters in the averaged I_{GABA} evoked in 2 mM $[Ca^{2+}]_o$ corresponding to the 20th–22nd averaged I_{GABA} became similar ($^{\dagger}P>0.9$ and $^{\dagger}P>0.2$, respectively) to those in the fifth–seventh averaged I_{GABA} at 2 mM $[Ca^{2+}]_o$ (Fig. 5Ad, Ae), compare open circles and gray triangles). Thus, the increase in the Ds was invariably accompanied by the increases in the Rs as well as half-duration in a

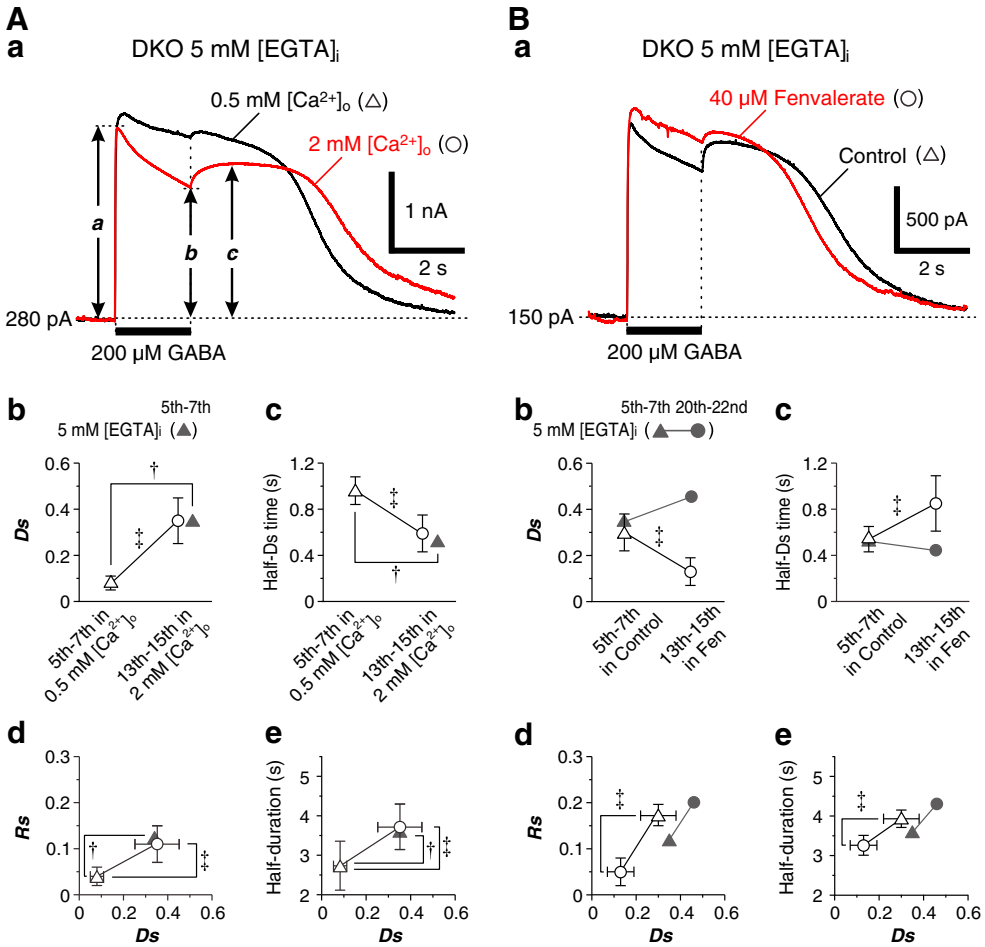

Fig. 5 Effects of $[Ca^{2+}]_o$ and fenvalerate on I_{GABA} in PRIP-DKO PCs. **A***a* Superimposed sample traces of the averaged I_{GABA} evoked by the fifth–seventh GABA puffs at 0 mV in 0.5 mM $[Ca^{2+}]_o$ and that evoked by the 13th–15th GABA puffs started after $[Ca^{2+}]_o$ was increased from 0.5 to 2 mM in a PRIP-DKO PC dialyzed with 5 mM EGTA. **A***b*, **A***c* The changes in the Ds (**A***b*) and half-Ds time (**A***c*) in the averaged I_{GABA} evoked by the fifth–seventh GABA puffs in 0.5 mM $[Ca^{2+}]_o$ (*open triangles*) and that evoked by the 13th–15th GABA puffs in 2 mM $[Ca^{2+}]_o$ (*open circles*). *Gray triangles* represent the respective mean values in the fifth–seventh averaged I_{GABA} at 2 mM $[Ca^{2+}]_o$ shown in Fig. 4C, D. ‡P<0.01, †P<0.01. **A***d*, **A***e* The relationships between the Ds and Rs (**A***d*) and between the Ds and half-duration of the tail-I (**A***e*). *Gray triangles* represent the respective relationships in the fifth–seventh averaged I_{GABA} at 2 mM $[Ca^{2+}]_o$ shown in Fig. 4E, F. ‡P<0.01, †P<0.01. **B***a* Superimposed sample traces of the averaged I_{GABA} evoked by the fifth–seventh GABA puffs in the control condition and that evoked by the 13th–15th GABA puffs started after application of 40 μM fenvalerate in a PRIP-DKO PC dialyzed with 5 mM EGTA. **B***b*, **B***c* The changes in the Ds (**B***b*) and half-Ds time (**B***c*) in the averaged I_{GABA} evoked by the fifth–seventh GABA puffs in the control condition and that evoked by the 13th–15th GABA puffs after fenvalerate (*Fen*) application. *Gray triangles* and *circles* represent the mean values in the fifth–seventh and the 20th–22nd averaged I_{GABA} at 2 mM $[Ca^{2+}]_o$, respectively, shown in Fig. 4C, D. ‡P<0.03. **B***d*, **B***e* The relationships between the mean Ds and Rs (**B***d*) and between the mean Ds and half-duration of the tail-I (**B***e*). *Gray triangles* and *circles* represent the relationships in the fifth–seventh and the 20th–22nd averaged I_{GABA} at 2 mM $[Ca^{2+}]_o$, respectively, shown in Fig. 4E, F. ‡P<0.02

manner dependent on $[Ca^{2+}]_o$ or $[Ca^{2+}]_i$, consistent with the observation shown in Fig. 4E, F (compare open and filled symbols). Taken together, it can be concluded that both the desensitization and resensitization of I_{GABA} at 0.5 mM $[Ca^{2+}]_o$ were weak due to a low $[Ca^{2+}]_o$, but became prominent after increasing $[Ca^{2+}]_o$ to 2 mM.

Effects of a calcineurin inhibitor on I_{GABA} in PRIP-DKO PCs

Because the alterations of I_{GABA} kinetics in PRIP-DKO PCs were mediated by high $[Ca^{2+}]_i$, we next investigated Ca^{2+}-dependent signal transduction involved in the alterations of I_{GABA} kinetics. It has been reported that the inhibition of calcineurin suppresses the desensitization of GABA currents in acutely dissociated hippocampal neurons [28] and increases the rate of GABA unbinding from $GABA_A$Rs in cultured hippocampal neurons [19]. Therefore, we examined whether and how fenvalerate, an inhibitor of calcineurin, modulates I_{GABA} in PRIP-DKO PCs dialyzed with 5 mM EGTA.

I_{GABA} was repeatedly evoked by seven trials of GABA puff application in the control condition and also repeatedly evoked by over 15 trials of GABA puff after bath application of 40 μM fenvalerate. Following application of fenvalerate for at least 15 min, the desensitization of I_{GABA} was alleviated,

while the hump-like tail-I after the puff offset was markedly decreased, as observed in the superimposed traces of the averaged I_{GABA} evoked by the fifth–seventh GABA puffs in the control condition and that evoked by the 13th–15th GABA puffs after fenvalerate application (Fig. 5Ba). When compared between these two averaged I_{GABA} evoked before and after fenvalerate application, the mean Ds and half-Ds time were significantly (n=5) decreased from 0.30±0.08 to 0.13±0.06 ($^{‡}P$<0.03) and increased from 0.54±0.11 to 0.85±0.24 s ($^{‡}P$<0.03), respectively (Fig. 5Bb, Bc). Both the Ds and half-Ds time in the averaged I_{GABA} evoked by the fifth–seventh GABA puffs in the control condition were not significantly ($^{†}P$>0.2 and $^{†}P$>0.6, respectively) different from those in the fifth–seventh averaged I_{GABA} shown in Fig. 4C, D (Fig. 5Bb, Bc, compare open and gray triangles), whereas the changes in these parameters caused by fenvalerate were opposite to the changes caused by the repeated application of GABA puff (Fig. 5Bb, Bc, compare open and gray symbols). These results suggest that the desensitization of I_{GABA} in PRIP-DKO PCs can be alleviated by calcineurin inhibition.

As seen in the scattergrams (Fig. 5Bd, Be), when compared between these two averaged I_{GABA} evoked before and after fenvalerate application, the mean Rs and half-duration were significantly (n=5) decreased from 0.17±0.02 to 0.05±0.03 ($^{‡}P$<0.01) and from 3.93±0.22 to 3.26±0.25 s ($^{‡}P$<0.02), respectively, along with the Ds. Thus, the decrease in the Ds was invariably accompanied by the decreases in the Rs as well as half-duration. These changes caused by fenvalerate were also opposite to the changes caused by the repeated application of GABA puff shown in Fig. 4E, F (Fig. 5Bd, Be, compare open and gray symbols). Taken together, these results suggest that the enhancement of desensitization of I_{GABA} and its subsequent resensitization, at least partly due to a slowdown of GABA-unbinding rate, in PRIP-DKO PCs are mediated by the higher endogenous activity of calcineurin, which might have been brought about by the higher $[Ca^{2+}]_i$, compared to WT PCs.

Effects of calcineurin on I_{GABA} in WT PCs

We next investigated whether or not calcineurin can induce a hump-like tail-I in WT PCs. In WT PCs dialyzed with 0.2 U/ml calcineurin and 5 mM EGTA (n=6), the I_{GABA} evoked 5 min after establishing the whole-cell configuration did not display a hump-like tail-I (Fig. 6Aa). However, 40 min after the whole-cell configuration, the normalized peak amplitude of I_{GABA} decreased significantly ($^{‡}P$<0.01) (Fig. 6Bb, open circles) and a hump-like tail-I emerged at the offset of the GABA puff (Fig. 6Aa). In contrast, in the WT PCs dialyzed with 5 mM EGTA alone (n=6), the normalized peak amplitude of I_{GABA} did not decrease markedly ($^{‡}P$>0.1) when compared between those obtained 5 and 40 min after the whole-cell configuration (Fig. 6Bb, filled circles) and the I_{GABA} never displayed a hump-like tail-I (Fig. 6Ba). The decrease in the normalized peak amplitude of I_{GABA} in WT PCs dialyzed with calcineurin and EGTA may be largely due to the desensitization caused by the activity of calcineurin. However, there were no significant differences in the mean Ds ($^{‡}P$>0.06) and half-Ds time ($^{‡}P$>0.6) between the I_{GABA} evoked 5 min and that evoked 40 min after the whole-cell configuration (Fig. 6Ab, Ac, open circles). This may be because $GABA_AR$ channels may had already been desensitized partly by the activity of calcineurin when the GABA puff was applied 40 min after the whole-cell configuration as reflected in the decrease in amplitude (Fig. 6Bb) and because the fraction of $GABA_AR$ channels available for further desensitization during the GABA puff might be small due to the limited activity of calcineurin brought about exogenously. However, the mean Rs and the mean half-duration were significantly ($^{‡}P$<0.01) increased (Fig. 6Ad, Ae, open circles). Thus, the activation of calcineurin enhanced the desensitization of I_{GABA} and slowed the GABA-unbinding rate (k_{off}), consistent with the findings in the previous reports [19, 28]. In the WT PCs dialyzed with 5 mM EGTA alone, there were no significant differences in the mean Ds ($^{‡}P$>0.8), the mean half-Ds time ($^{‡}P$>0.4), and the mean half-duration ($^{‡}P$>0.7) between the I_{GABA} evoked 5 min and that evoked 40 min after the whole-cell configuration (Fig. 6Ab, Ac, Ae), filled circles). The mean half-duration of the tail-I was significantly ($^{†}P$<0.01) longer in the WT PCs dialyzed with calcineurin and EGTA than in those dialyzed with EGTA alone when examined 40 min after the whole-cell configuration (Fig. 6Ae), reflecting the presence of hump-like tail-Is. Taken together, these results strongly suggest that calcineurin is really required to induce the hump-like tail-I.

Effects of ruthenium red on I_{GABA} in PRIP-DKO PCs

The enhanced desensitization and resensitization of I_{GABA} in PRIP-DKO PCs are likely to be mediated by the higher $[Ca^{2+}]_i$. It is possible that the increases in $[Ca^{2+}]_i$ are brought about either by the potentiated CICR due to the impairment of IICR in the shared Ca^{2+} store as shown in PRIP-1 KO mice [9] and/or by the enhanced SOCE as demonstrated in PRIP-2 KO mice [40]. Therefore, we next investigated the possible involvements of CICR and the subsequent SOCE in inducing the desensitization and resensitization of I_{GABA}, by examining whether and how I_{GABA} evoked in PRIP-DKO PCs can be modulated by the intracellular application of ruthenium red that blocks CICR [10, 29]. With the repetition of GABA puff applications for 2 s every minute, the desensitization of I_{GABA} evoked in PRIP-DKO PCs dialyzed with 100 μM ruthenium red and 5 mM EGTA was progressively alleviated while the hump-like tail-I after the puff offset was progressively suppressed, as observed in the superimposed traces of the fifth and the 22nd I_{GABA} (Fig. 7A).

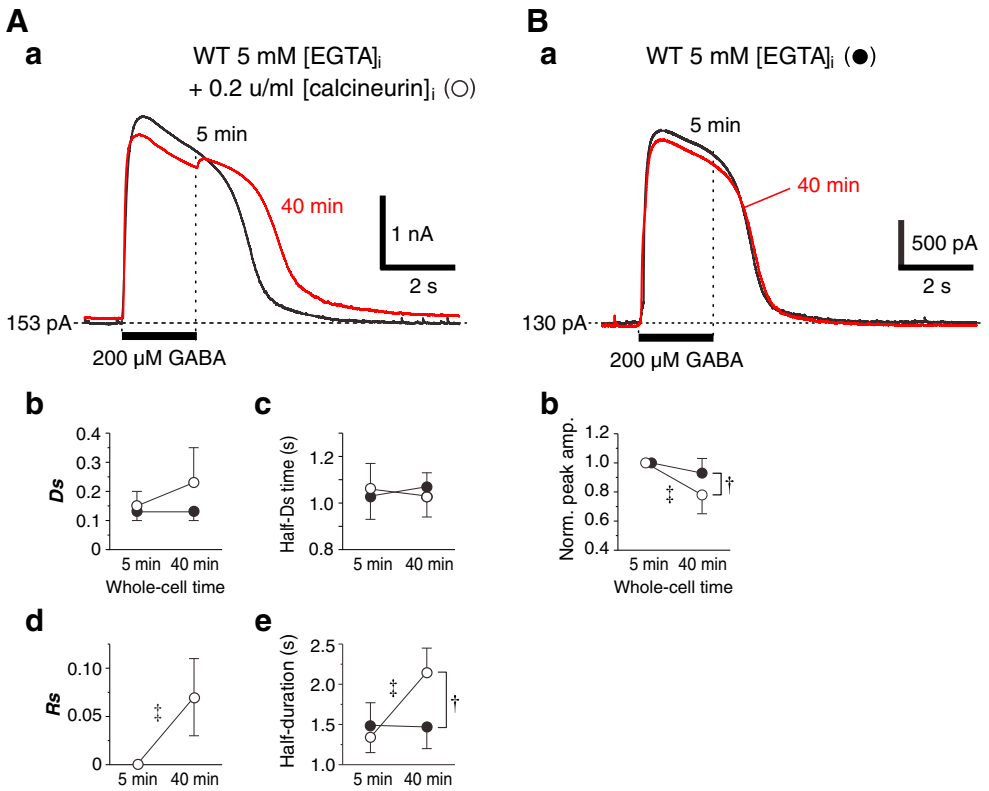

Fig. 6 Effects of calcineurin on I_{GABA} in WT PCs. **A***a* Superimposed sample traces of I_{GABA} recorded 5 and 40 min after the whole-cell configuration in a WT PC dialyzed with 0.2 U/ml calcineurin and 5 mM EGTA. **A***b* The mean Ds in I_{GABA} recorded 5 and 40 min after the whole-cell configuration in WT PCs dialyzed with 5 mM EGTA alone (*filled circles*: 0.13±0.03 and 0.13±0.04, respectively, n=6) and in those dialyzed with calcineurin and EGTA (*open circles*: 0.15±0.05 and 0.23±0.12, respectively, n=6). **A***c* The mean half-Ds time in I_{GABA} recorded 5 and 40 min after the whole-cell configuration in WT PCs dialyzed with EGTA alone (*filled circles*: 1.03±0.11 and 1.07±0.06 s, respectively, n=6) and in those dialyzed with calcineurin and EGTA (*open circles*: 1.06±0.12 and 1.03±0.10 s, respectively, n=6). **A***d* The change in the Rs in the I_{GABA} recorded 5 and 40 min after the whole-cell configuration in WT PCs dialyzed with calcineurin and EGTA (0.001±0.002 and 0.07±0.04, respectively, n=6). $^{‡}P$<0.01. **A***e* The mean half-duration in I_{GABA} recorded 5 and 40 min after the whole-cell configuration in WT PCs dialyzed with EGTA alone (*filled circles*: 1.49±0.30 and 1.47±0.30 s, respectively, n=6) and in those dialyzed with calcineurin and EGTA (*open circles*: 1.34±0.20 and 2.15±0.33 s, respectively, n=6). $^{‡}P$<0.01, $^{†}P$<0.01. **B***a* Superimposed sample traces of I_{GABA} recorded 5 and 40 min after the whole-cell configuration in a WT PC dialyzed with 5 mM EGTA alone. **B***b* Normalized peak amplitudes of I_{GABA} recorded 5 and 40 min after the whole-cell configuration in WT PCs dialyzed with calcineurin and EGTA (*open circles*) and in those dialyzed with EGTA alone (*filled circles*). $^{‡}P$<0.01, $^{†}P$<0.05

The mean Ds in the 20th–22nd averaged I_{GABA} (0.17±0.04) was significantly ($^{‡}P$<0.02, n=5) smaller than that in the fifth–seventh averaged I_{GABA} (0.27±0.05) (Fig. 7B), and the mean half-Ds time was significantly ($^{‡}P$<0.01, n=5) longer in the 20th–22nd averaged I_{GABA} (0.65±0.05 s) compared to the fifth–seventh averaged I_{GABA} (0.50±0.07 s) (Fig. 7C). Both the Ds and half-Ds time in the control condition were not significantly ($^{†}P$>0.06 and $^{†}P$>0.6, respectively) different from those in the fifth–seventh averaged I_{GABA} shown in Fig. 4C, D (Fig. 7B, C, compare open and gray triangles) whereas the changes in these parameters following intracellular diffusion of ruthenium red were opposite to the changes caused by the repeated application of GABA puff (Fig. 7B, C, compare open and gray symbols). These results clearly indicate that the desensitization of I_{GABA} in PRIP-DKO PCs was markedly alleviated in the presence of intracellular ruthenium red. As a consequence of the alleviation of I_{GABA} desensitization by ruthenium red, the Rs was significantly ($^{‡}P$<0.02, n=5) decreased from 0.13±0.04 to 0.06±0.03 along with the Ds following the repetition of puff applications of GABA from the fifth–seventh trials to the 20th–22nd trials (Fig. 7D). Thus, the decrease in Rs invariably accompanied the decrease in the Ds following intracellular diffusion of ruthenium red. Similarly, a significant shortening of the half-duration of the hump-like tail-I in the 20th–22nd averaged I_{GABA} (3.57±0.74 s) from that in the fifth–seventh averaged I_{GABA} (4.02±0.71 s) (Fig. 7E, $^{‡}P$<0.01, n=5) accompanied the decrease in the Ds. These changes caused by ruthenium red were also opposite to the changes caused by the repeated application of GABA puff shown in Fig. 4E, F (Fig. 7D, E, compare open and gray symbols). These results suggest that the enhanced desensitization and resensitization of I_{GABA} in PRIP-DKO PCs are largely induced by increases in $[Ca^{2+}]_i$ through CICR and/or the subsequent SOCE.

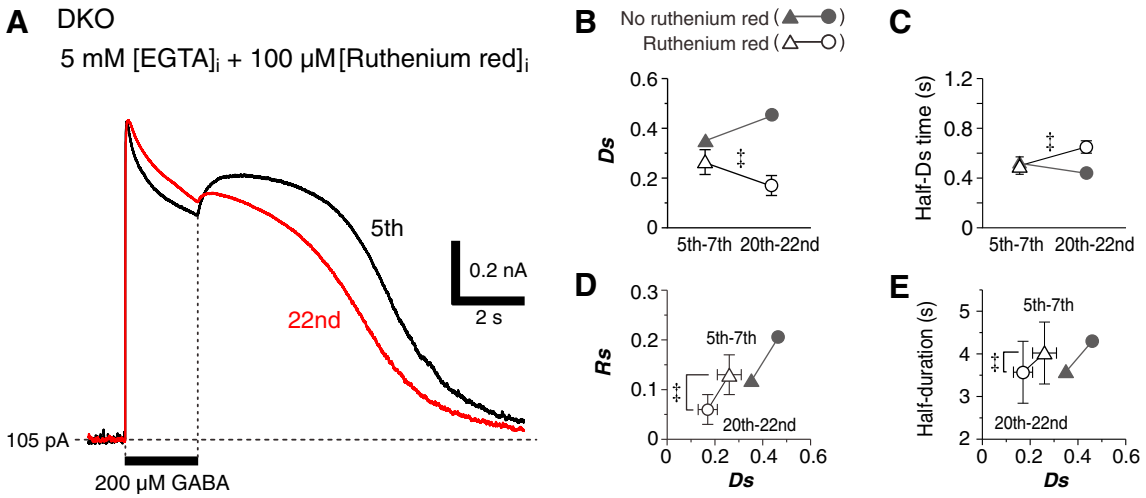

Fig. 7 Enhanced desensitization and resensitization of I_{GABA} in PRIP-DKO PCs are induced by CICR. **A** Sample traces of the fifth and the 22nd I_{GABA} in PRIP-DKO PCs dialyzed with 100 μM ruthenium red and 5 mM EGTA. **B**, **C** The changes in the Ds (**B**) and half-Ds time (**C**) in the fifth–seventh (*open triangles*) and the 20th–22nd averaged I_{GABA} (*open circles*). *Gray triangles* and *circles* represent the mean values in the fifth–seventh and the 20th–22nd averaged I_{GABA} at 2 mM $[Ca^{2+}]_o$, respectively, shown in Fig. 4C, D. ‡$P<0.02$. **D**, **E** The relationships between the Ds and Rs (**D**) and between the Ds and half-duration (**E**) in the fifth–seventh (*open triangles*) and the 20th–22nd averaged I_{GABA} (*open circles*). *Gray triangles* and *circles* represent the relationships in the fifth–seventh and the 20th–22nd averaged I_{GABA} at 2 mM $[Ca^{2+}]_o$, respectively, shown in Fig. 4E, F. ‡$P<0.02$

Although ruthenium red blocks not only CICR but also various Ca^{2+} channels such as TRP channels [43] and voltage-gate Ca^{2+} channels [6], ruthenium red at least blocks CICR. This is because the blockade of Ca^{2+} channels may result in the blockade of CICR. Provided that CICR is involved in the enhanced desensitization and the subsequent resensitization of I_{GABA} observed in PRIP-DKO PCs but not in WT PCs, CICR should be more potent in PRIP-DKO PCs than in WT PCs. In the next experiment, we examined whether or not CICR and the subsequent SOCE differ between WT and PRIP-DKO PCs using a Ca^{2+}-imaging method.

Apparent enhancement of CICR in PRIP-DKO PCs

Changes in $[Ca^{2+}]_i$ were measured in visually identified L3 PCs in slice preparations incubated with 10 μM fura-2 AM (Fig. 8A). Usually, Ca^{2+} images were captured simultaneously in two to four cells in the same slices (Fig. 8Ba, Da). These cells displayed similar Ca^{2+} transients in response to a brief (3 min) application of high-K^+ (20 mM) solution or a brief (3 min) application of 20 mM caffeine followed by a brief (3 min) application of the mixed solution of 20 mM K^+ and 20 mM caffeine (the combined application of the caffeine and the mixed solutions). In a slice preparation obtained from PRIP-DKO mice, the two PCs in the same slice (Fig. 8Ba, single and double arrowheads) displayed similar large Ca^{2+} transients in response to the brief application of the high-K^+ solution, while the combined application of the caffeine and the mixed solutions 5 min after washout of the preceding high-K^+ solution induced only small increases in $[Ca^{2+}]_i$ (Fig. 8Bb). A similar observation has been made in nine of 10 PRIP-DKO slices examined. In contrast, in the remaining one of the 10 slices, the brief application of high-K^+ solution induced small Ca^{2+} transients while the subsequent combined application of the caffeine and the mixed solutions induced large Ca^{2+} transients simultaneously in the three PCs as represented by the three superimposed traces of similar Ca^{2+} transients (Fig. 8Bc). In a slice preparation obtained from WT mice, the brief application of the high-K^+ solution induced similar large Ca^{2+} transients while the subsequent combined application of the caffeine and the mixed solutions induced only small increases in $[Ca^{2+}]_i$, in three PCs as represented by the three superimposed traces of Ca^{2+} transients (Fig. 8C). A similar observation has been made in eight of eight WT slices examined. The amplitude of Ca^{2+} transients was measured as a difference in the F_{340}/F_{380} ratio from the baseline level. There was no significant (†$P>0.9$) difference in the mean peak amplitude of Ca^{2+} transients induced by the brief application of high-K^+ solution between the PRIP-DKO (1.12±0.10, $n=9$) and WT PCs (1.11±0.18, $n=8$).

Provided that the first application of the high-K^+ solution induced CICR, the subsequent combined application of the caffeine and the mixed solutions may have failed to induce CICR due to the preceding depletion of Ca^{2+} stores. Thus, a large Ca^{2+} transient is likely to be induced by CICR. Because the sole application of the high-K^+ solution failed to induce CICR although in one of 10 PRIP-DKO slices, the high-K^+ solution was applied in the presence of the caffeine solution to securely induce CICR. Indeed, the persistent application of the high-K^+ solution that was preceded by 3 min by the persistent application of 20 mM caffeine invariably induced large Ca^{2+} transients. In a slice preparation obtained from PRIP-DKO mice,

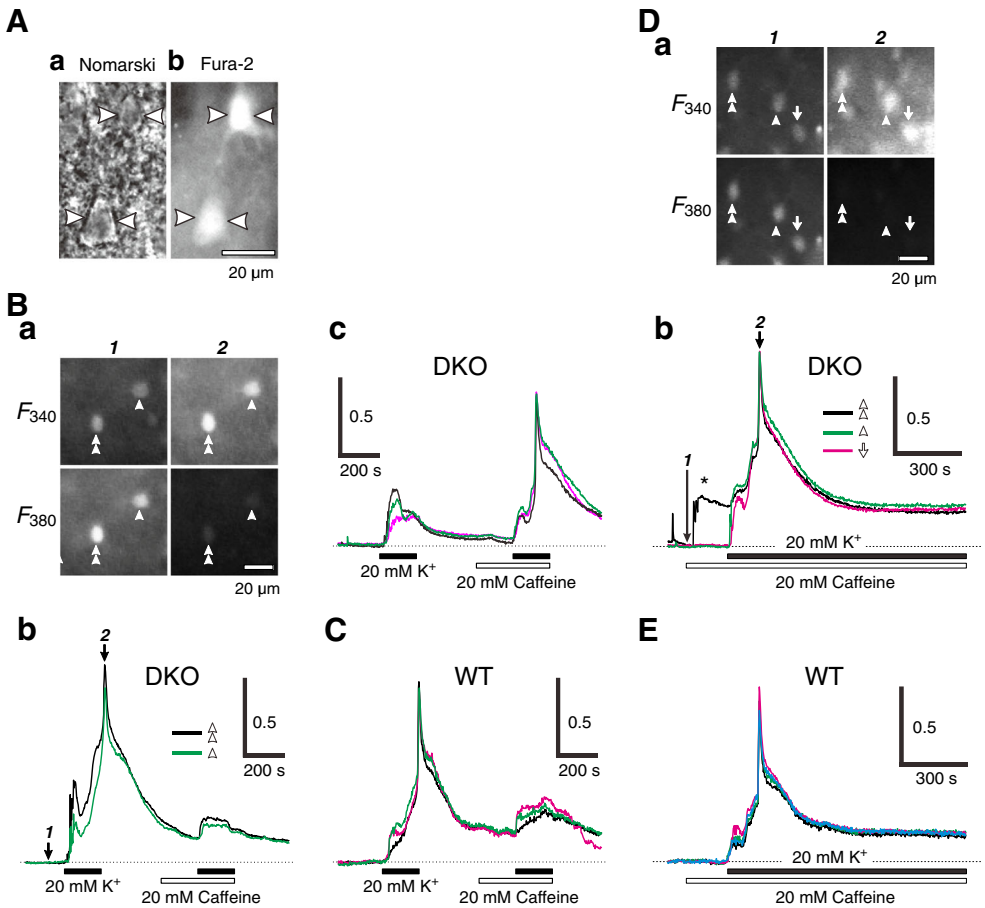

Fig. 8 Comparison of CICR between WT and PRIP-DKO PCs. **A***a*, **A***b* Photomicrographs showing a Nomarski (**A***a*) and fura-2 fluorescence image (**A***b*, F_{340}) of the same two L3 PRIP-DKO PCs indicated with *arrowheads*. **B***a* Sample F_{340} and F_{380} images of the two PCs (indicated with *single* and *double arrowheads*) in a PRIP-DKO slice obtained before (*1*) and at the peak time of CICR (*2*), which are indicated with *1* and *2* in the Ca^{2+} transients representing the F_{340}/F_{380} ratio (**B***b*). **B***b* Ca^{2+} transients showing CICR in response to application of the high-K^+ (20 mM) solution in the two PCs in a PRIP-DKO slice, which are indicated with *single* and *double arrowheads* in (**B***a*). No CICR in response to the subsequent combined application of the caffeine and the mixed solutions. **B***c* Small responses to the high-K^+ solution followed by CICR induced in response to the subsequent combined application of the caffeine and the mixed solutions in three PCs in a PRIP-DKO slice. **C** CICR induced in response to the high-K^+ solution followed by small responses to the subsequent combined application of the caffeine and the mixed solutions in three PCs in a WT slice. **D***a* Sample F_{340} and F_{380} images of the three PCs (indicated with *single* and *double arrowheads* and *arrow*) in a PRIP-DKO slice obtained before (*1*) and at the peak time of CICR (*2*), which are indicated with *1* and *2* in the Ca^{2+} transients representing the F_{340}/F_{380} ratio (**D***b*). **D***b* Ca^{2+} transients showing CICR in response to the combined persistent application of the caffeine and the mixed solutions in the three PCs in a PRIP-DKO slice, which are indicated with *single* and *double arrowheads* and *arrow* in **D***a*. An asterisk indicates a small Ca^{2+} transient observed during the 20-mM caffeine solution alone period. **E** CICR induced in response to the combined persistent application of the caffeine and the mixed solutions in four PCs in a WT slice

the three PCs in the same slice (Fig. 8Da, single and double arrowheads and arrow) displayed similar large Ca^{2+} transients in response to the combined persistent application the caffeine and the mixed solutions, which decayed to a plateau level (Fig. 8Db). Similar observation was made in WT PCs (Fig. 8E). Such a plateau of $[Ca^{2+}]_i$ caused by the combined persistent application of the caffeine and the mixed solutions was maintained at least for 10 min examined (Fig. 8Db, De). The mean peak and plateau amplitudes of Ca^{2+} transients induced by the combined persistent application in the PRIP-DKO PCs (1.19±0.09 and 0.32±0.02, respectively, n=6) were significantly ($^{\dagger}P$<0.03 and $^{\dagger}P$<0.02, respectively) larger than those in the WT PCs (1.00±0.13 and 0.22±0.05, respectively, n=5). However, 20 mM caffeine alone neither induced CICR nor affected the baseline level of $[Ca^{2+}]_i$ in PCs in 11 of 17 PRIP-DKO slices examined and in 13 of 18 WT slices examined while it induced only a small Ca^{2+} transient in the remaining six PRIP-DKO and five WT slices, similar to a small $[Ca^{2+}]_i$ increase observed during the caffeine alone period in the combined application of the caffeine and the mixed solutions (Fig. 8Db, *). These effects of caffeine were consistent with the previous report in cultured hippocampal neurons [38]. Because CICR is known to be followed by SOCE [7, 34], these results suggest that Ca^{2+} entry occurred following the depletion of Ca^{2+} stores by CICR [34].

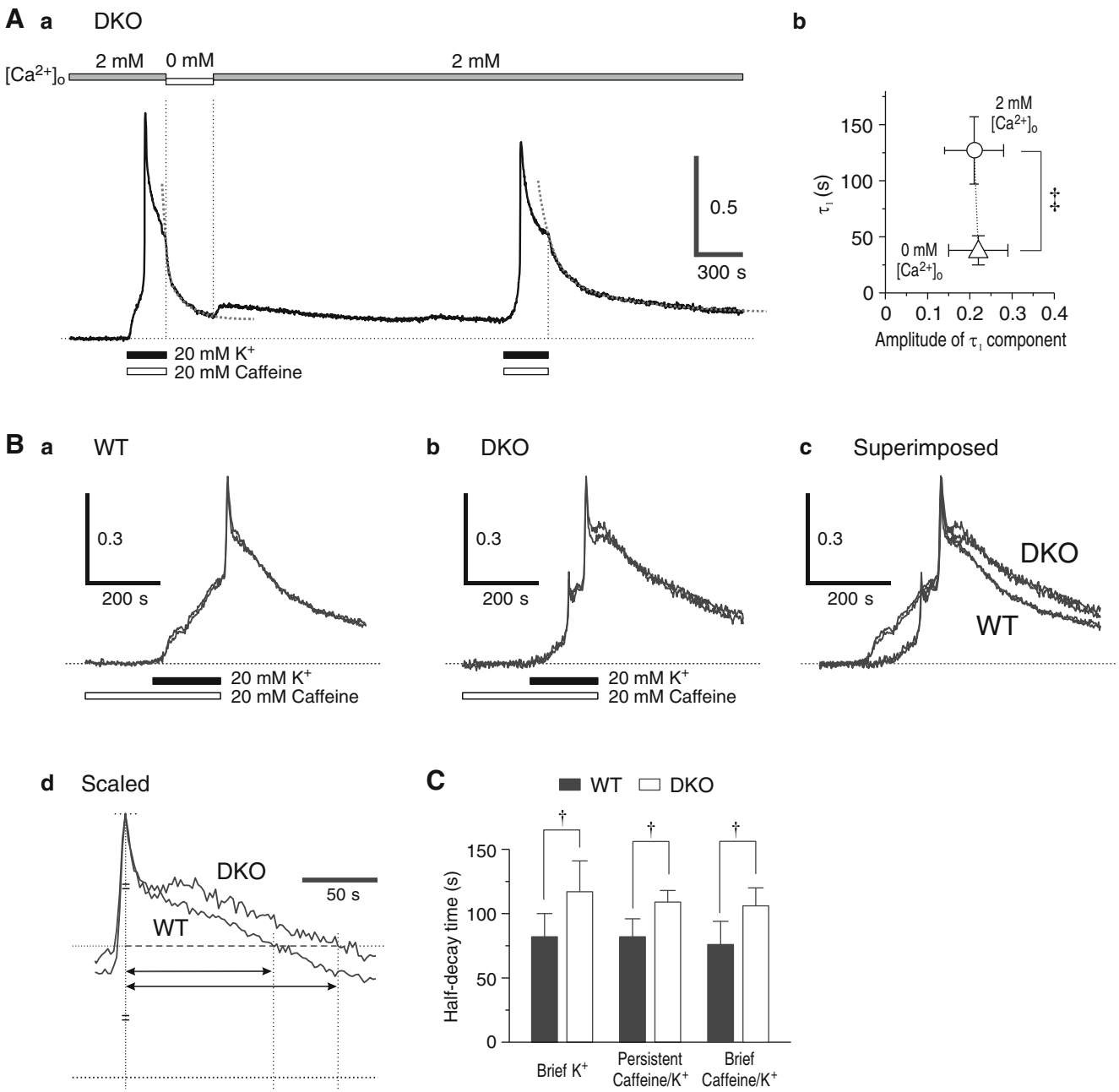

Fig. 9 Enhancement of SOCE in PRIP-DKO PCs. **A***a* A rapid decay of the F_{340}/F_{380} ratio following the first CICR after $[Ca^{2+}]_o$ was decreased to zero and a slow decay following the second CICR when $[Ca^{2+}]_o$ was maintained at 2 mM. The *dotted gray curves* represent double exponential curves that describe the decay of the F_{340}/F_{380} ratio. **A***b* An acceleration of τ_1 without changes in the initial amplitude following a decrease in $[Ca^{2+}]_o$ from 2 (*circle*) to 0 mM (*triangle*). $^{\ddagger}P<0.01$. **B***a*, **B***b* Two superimposed traces of Ca^{2+} transients obtained from two PCs in a WT slice (**B***a*) and those of Ca^{2+} transients obtained from two PCs in a PRIP-DKO slice (**B***b*) in response to the combined application of the caffeine and the mixed solutions which were washed out immediately after CICR. **B***c* Superimposed traces of Ca^{2+} transients shown in **B***a* and **B***b*. After washout of the combined application of the caffeine and the mixed solutions, the F_{340}/F_{380} ratio decayed differently between PCs in WT and PRIP-DKO slices. **B***d* Superimposed scaled traces of Ca^{2+} transients recorded from WT and PRIP-DKO PCs, indicating a slower decay from the peak in the PRIP-DKO PC compared to the WT. *Double-headed arrows* represent the half-decay times from the peak of CICR. **C** The mean half-decay times from the peak CICR induced in response to the brief application of the high-K^+ solution (brief K^+), the combined persistent application of the caffeine and the mixed solutions (persistent caffeine/K^+) and the combined application of the caffeine and the mixed solutions (brief caffeine/K^+) in PCs in WT (filled columns) and PRIP-DKO (open columns) slices. $^{\dagger}P<0.02$

Enhanced SOCE in PRIP-DKO PCs

In PRIP-DKO PCs, whether SOCE occurred following CICR or not was directly examined by reducing $[Ca^{2+}]_o$. The CICR was induced twice consecutively by the first and second applications of the mixed solution of 20 mM caffeine and 20 mM K^+ (caffeine/high-K^+ solution), which were separated by 35–40 min (Fig. 9Aa). Immediately after the first and second CICR, the caffeine/high-K^+ solution was changed to the Ca^{2+}-free extracellular solution and the standard extracellular solution containing 2 mM Ca^{2+}, respectively. Compared to the decrease in the F_{340}/F_{380} ratio observed during the application of standard extracellular solution containing 2 mM Ca^{2+} following the second CICR, the F_{340}/F_{380} ratio appeared to decrease more steeply during the application of the Ca^{2+}-free extracellular solution following the first CICR and increased immediately after $[Ca^{2+}]_o$ was increased from 0 to 2 mM (Fig. 9Aa). The decay time course of the F_{340}/F_{380} ratio was fitted with a double exponential curve and was compared between the responses obtained in the two extracellular solutions. The fast decay time constant (τ_1) was significantly smaller ($^{\ddagger}P<0.01$, $n=6$) in the responses to the change to 0 mM $[Ca^{2+}]_o$ (38±13 s) compared to those to 2 mM $[Ca^{2+}]_o$ (127±30 s) whereas there was no significant ($^{\ddagger}P>0.6$, $n=6$) difference in the amplitude of the F_{340}/F_{380} ratio (0.22±0.07 and 0.21±0.07, respectively) that decreases with the τ_1 (Fig. 9Ab). These observations would clearly indicate that CICR was followed by SOCE.

Next, we examined whether the SOCE following the potentiated CICR in PRIP-DKO PCs is more potent compared to the WT. When Ca^{2+} transients were induced by the combined application of the caffeine and the mixed solutions, it decayed differently between PCs in PRIP-DKO and WT slices (Fig. 9Ba–c) as reflected in the half-decay time (Fig. 9Bd, compare the respective double-headed arrows), to a low $[Ca^{2+}]_i$ level from which it further decayed with a similar slow time course (Fig. 9Ba–c). The mean half-decay time from the peak CICR was significantly longer in the PRIP-DKO PCs than in the WT PCs, irrespective of the responses to the brief application of the high-K^+ solution (WT 82±18 s, $n=8$; PRIP-DKO 117±24 s, $n=9$; $^{\dagger}P<0.01$) or those to the combined persistent application of the caffeine and the mixed solutions (WT 82±14 s, $n=6$; PRIP-DKO 109±9 s, $n=5$; $^{\dagger}P<0.02$) or those to the combined application of the caffeine and the mixed solutions (WT 76±18 s, $n=6$; PRIP-DKO 106±14 s, $n=6$; $^{\dagger}P<0.02$) (Fig. 9C). Because SOCE occurs following CICR [34] as demonstrated in Fig. 8D, these results strongly suggest that both the CICR and the subsequent SOCE are more potent in PRIP-DKO PCs than in WT PCs.

Discussion

In the present study, we showed that the deletion of PRIP-1/2 accelerated the desensitization of I_{GABA} but caused a hump-like tail-I at the offset of the GABA puff (Figs. 1, 4, and 5). The enhancement of desensitization and resensitization of $GABA_A$Rs in PRIP-DKO PCs was mediated by the enhanced activity of Ca^{2+}-dependent calcineurin through the potentiated CICR and SOCE. To the best of our knowledge, there has been no report on such hump-like tail-Is that are induced by GABA itself, although similar tail-Is were observed following the removal of anesthetic drugs such as propofol [36] and pentobarbital [1, 2].

$[Ca^{2+}]_i$ dependence of I_{GABA} desensitization and resensitization and their abolishment by a calcineurin inhibitor

It was clearly demonstrated that both the acceleration of I_{GABA} desensitization and the generation of the hump-like tail-I were brought about by increases in $[Ca^{2+}]_i$, as revealed by changes in $[Ca^{2+}]_o$ from 0.5 to 2 mM (Fig. 5A) and by changes in $[EGTA]_i$ from 10 to 5 mM (Fig. 4). Consistent with the idea that desensitization is mechanistically related to the deactivation in $GABA_A$Rs [18], the progress of desensitization of I_{GABA} was invariably accompanied by the enhancement of the hump-like tail-I (Figs. 4 and 5A). These results suggest that the deletion of PRIP-1/2 results in an enhancement of the desensitization and resensitization of $GABA_A$Rs through increases in $[Ca^{2+}]_i$. The involvement of CICR and the following SOCE in both the desensitization of I_{GABA} and the generation of the hump-like tail-I in PRIP-DKO PCs was also demonstrated by the intracellular application of ruthenium red (Fig. 7).

It has been demonstrated that the desensitization of $GABA_A$Rs was enhanced by increases in $[Ca^{2+}]_i$ [15, 33] and that a calcineurin inhibitor, cyclosporin A-cyclophilin A complex, suppressed the desensitization of GABA currents in acutely dissociated hippocampal neurons [28]. It has also been reported that the inhibition of calcineurin increased the rate of GABA unbinding from $GABA_A$Rs [19]. Consistent with these previous studies, the bath application of fenvalerate alleviated the desensitization of I_{GABA} and markedly decreased the hump-like tail-I in the present study (Fig. 5B). Thus, it is likely that the hump-like tail-I in PRIP-DKO PCs was generated as a result of an acceleration of desensitization of I_{GABA} coupled with a slowdown of the GABA unbinding, which was mediated by Ca^{2+}-dependent activation of calcineurin. In support of this idea, it was observed that an injection of calcineurin in

WT PCs induced a hump-like tail-I (Fig. 6). Because CICR and the following SOCE were more potent in PRIP-DKO PCs than in WT PCs (Figs. 8 and 9), these results strongly suggest that the enhancement of desensitization and resensitization of $GABA_A$Rs in PRIP-DKO PCs was largely mediated by the upregulation of Ca^{2+}-dependent activity of calcineurin due to the potentiation of CICR followed by SOCE.

A possible mechanism for the higher $[Ca^{2+}]_i$ in PRIP-DKO PCs

There is evidence that ryanodine and IP_3 receptors share a common functional Ca^{2+} pool in cultured rat cerebellar granule [17], acutely dissociated rat hippocampal [14], rat cerebellar Purkinje [24], and rat neocortical neurons [27]. As the affinity of PRIP-1 for IP_3 is higher than that of PRIP-2 [41], the hydrolysis of IP_3 is suppressed more by PRIP-1 compared to PRIP-2. Therefore, the impairment of IICR was largely caused by the deletion of PRIP-1 in cultured cortical neurons [9]. Then, CICR may have been potentiated due to the impairment of IICR in the shared Ca^{2+} pool in PRIP-1 KO mice. On the other hand, it has also been reported that the SOCE was enhanced in hematopoietic B cells in PRIP-2 KO mice [40]. The SOCE that is regulated by the filling state of endoplasmic reticulum (ER) Ca^{2+} stores is an important Ca^{2+} influx pathway in non-excitable and excitable cells [7]. The Ca^{2+} sensor stromal interacting molecules (STIMs) localized in the ER sense the Ca^{2+} concentration of ER and activate Ca^{2+} release-activated Ca^{2+} (CRAC) channel upon the depletion of internal Ca^{2+} following IICR or CICR by binding to the CRAC protein 1 (CRACM1 or Orai1) [7]. This has also been demonstrated in cultured cortical neurons [8]. In view of these findings, the deletion of PRIP-2 may cause the higher activity of STIMs and Orai1 and thereby increase the activity of SOCE. Taken together, it is possible that the higher $[Ca^{2+}]_i$ in PRIP-DKO PCs is mediated by the enhancement of CICR and the following enhanced SOCE through the deletion of PRIP-1 and PRIP-2, respectively. However, further studies are apparently required to clarify how the deletion of PRIP-2 affects the activity of STIMs and Orai1 in L3 PCs of the barrel cortex.

A possible kinetic mechanism underlying the generation of the hump-like tail-I

We simulated the I_{GABA} followed by a hump-like tail-I using a model previously proposed (Fig. 10A [18]) to examine whether the possible increase in the fast desensitization rate (d_2) and the possible decrease in the unbinding rate (k_{off}) can lead to a generation of the hump-like tail-I at the offset of the GABA puff. It has been reported that after $GABA_A$Rs had been desensitized by application of GABA, GABA binding was greatly increased in the desensitized $GABA_A$Rs compared to the non-desensitized $GABA_A$Rs, and the binding increase was dependent on the concentration of the pre-applied GABA as was the case with the degree of desensitization of GABA

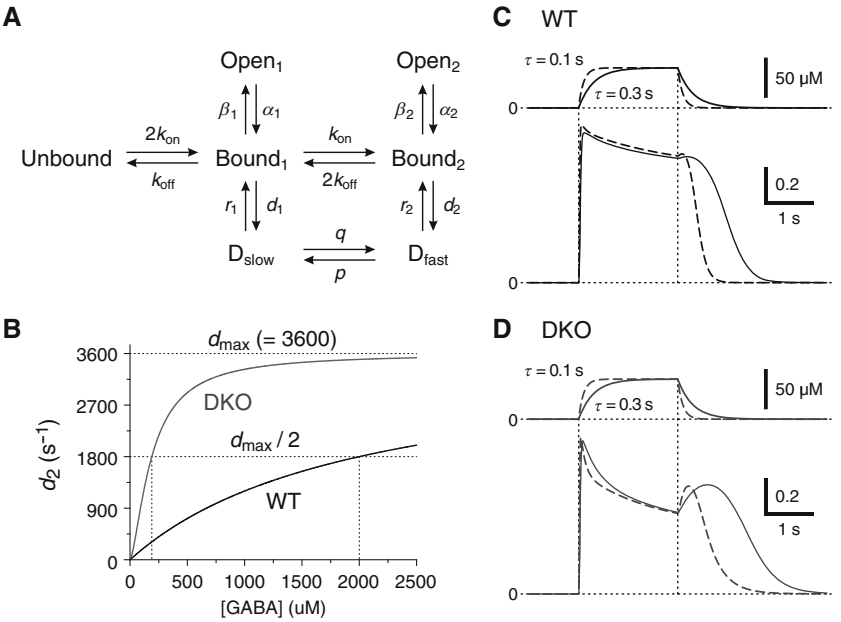

Fig. 10 A kinetic model for a hump-like tail-I. **A** A kinetic model of $GABA_A$Rs representing mono- and double-liganded states, each providing access to open and desensitized states. **B** Hypothesized GABA concentration ([GABA])-dependent changes of d_2 in WT and PRIP-DKO $GABA_A$Rs. **C**, **D** *Top*: presumed [GABA] changes during puff application of GABA. Two hundred micromolars GABA applied by a rectangular pressure pulse was assumed to be diluted four times in the extracellular solution, and the onset and offset of the puff application were assumed to be attenuated with a time constant raging between 0.1 and 0.3 s. *Bottom*: superimposed traces of the simulated I_{GABA} under the condition that the attenuation time constant is 0.3 and 0.1 s (*solid* and *interrupted traces*, respectively) in simulated WT (**C**) and PRIP-DKO PCs (**D**)

currents [4]. Then, when the probability of being in the desensitized state (D_{fast}) for $GABA_A$Rs was increased by increasing GABA concentration ([GABA]) or during the 2-s puff application of GABA, D_{fast} would be recruited more compared to $Open_2$. Thus, it is likely that the d_2, but not β_2, would increase in a manner dependent on [GABA] (Fig. 10B). Because $Bound_2$ that is bifurcated into $Open_2$ and D_{fast} increases in a manner dependent on [GABA] in the present model, we incorporated the idea in the present model by defining d_2 as follows:

$$d_2 = \frac{d_{max}}{1 + \left(\frac{K_h}{[GABA]}\right)^n}$$

where d_{max} is the maximum desensitization rate, K_h is the [GABA] that yields the half maximum desensitization rate, and n is the Hill coefficient. The [GABA] dependence of d_2 can be enhanced by an increase in n and a decrease in K_h (Fig. 10B). We assumed that calcineurin increased d_2 by increasing the [GABA] dependency of the desensitization rate and the d_2 and k_{off} were changed between the simulated WT and PRIP-DKO PCs. These changes were comparable to those caused by activation of calcineurin reported previously [19, 28].

When GABA puff was applied by a rectangular pressure pulse through a puff pipette containing 200 μM GABA, the ejected GABA was assumed to be diluted four times in the extracellular solution, and the onset and offset of the puff application were assumed to be attenuated with a time constant raging between 0.1 and 0.3 s. In the simulated WT PC where k_{off}=90, d_{max}=3,600, K_h=2,000 μM, and n=1, I_{GABA} was induced without a hump-like tail-I in response to 2-s GABA puff at 50 μM (Fig. 10C). In contrast, in the simulated PRIP-DKO PC where k_{off}=30 and d_{max} were the same as those in WT, K_h=200 μM, and n=1.5, I_{GABA} displayed a prominent desensitization and was followed by a prominent hump-like tail-I (Fig. 10D). Thus, by assuming a slowdown of k_{off} and an acceleration of d_2 through an increase in n and a decrease in K_h, a hump-like tail-I could be induced. At the offset of GABA puff, a sharp decrease in d_2 to a level smaller than the fast resensitization rate constant (r_2) occurred to subsequently induce a hump-like tail-I. Decreases in the decay time constant at the offset of GABA puff pulse from 0.3 to 0.1 s decreased the half-duration of the hump-like tail-I, leaving its amplitude or Rs almost unchanged (Fig. 10D). Only PRIP-DKO PCs but not WT PCs displayed hump-like tail-Is in response to the same GABA puff that may have decayed slowly. These observations clearly indicate that the generation of the hump-like tail-I reflects kinetic differences between $GABA_A$Rs in WT and PRIP-DKO PCs. Taken together, it was suggested that a higher calcineurin activity in PRIP-DKO L3 PCs might have caused a slowdown of k_{off} and an acceleration of d_2 through the modulation of its GABA concentration dependency, leading to a generation of hump-like tail-Is in PRIP-DKO PCs.

Acknowledgments The authors thank Dr. N. Akaike for critically reviewing an earlier version of the manuscript. This study was supported by a Grant-in-Aid for Scientific Research to Y.K. (B; 22300127) and that to M.H. (S; 24229009) from Japan Ministry of Education, Culture, Sports, Science and Technology.

Conflict of interest Authors declare no conflict of interest.

References

1. Akaike N, Hattori K, Inomata N, Oomura Y (1985) γ-Aminobutyric-acid- and pentobarbitone-gated chloride currents in internally perfused frog sensory neurones. J Physiol 360:367–386, PMID: 2580971
2. Akaike N, Maruyama T, Tokutomi N (1987) Kinetic properties of the pentobarbitone-gated chloride current in frog sensory neurones. J Physiol 394:85–98, PMID: 3502144
3. Bormann J, Hamill OP, Sakmann B (1987) Mechanism of anion permeation through channels gated by glycine and γ-aminobutyric acid in mouse cultured spinal neurones. J Physiol 385:243–286, PMID: 2443667
4. Chang Y, Ghansah E, Chen Y, Ye J, Weiss DS (2002) Desensitization mechanism of GABA receptors revealed by single oocyte binding and receptor function. J Neurosci 22:7982–7990, PMID: 12223551
5. Chen QX, Wong RK (1995) Suppression of $GABA_A$ receptor responses by NMDA application in hippocampal neurones acutely isolated from the adult guinea-pig. J Physiol 482:353–362, PMID: 7714826
6. Cibulsky SM, Sather WA (1999) Block by ruthenium red of cloned neuronal voltage-gated calcium channels. J Pharmacol Exp Ther 289:1447–1453, PMID: 10336538
7. Feske S (2010) CRAC channelopathies. Pflugers Arch 460:417–435. doi:10.1007/s00424-009-0777-5, PMID: 20111871
8. Gruszczynska-Biegala J, Pomorski P, Wisniewska MB, Kuznicki J (2011) Differential roles for STIM1 and STIM2 in store-operated calcium entry in rat neurons. PLoS One 6:e19285. doi:10.1371/journal.pone.0019285, PMID: 21541286
9. Harada K, Takeuchi H, Oike M, Matsuda M, Kanematsu T, Yagisawa H, Nakayama KI, Maeda K, Erneux C, Hirata M (2005) Role of PRIP-1, a novel $Ins(1,4,5)P_3$ binding protein, in $Ins(1,4,5)P_3$-mediated Ca^{2+} signaling. J Cell Physiol 202:422–433. doi:10.1002/jcp.20136, PMID: 15468068
10. Henzi V, MacDermott AB (1992) Characteristics and function of Ca^{2+}- and inositol 1,4,5-trisphosphate-releasable stores of Ca^{2+} in neurons. Neuroscience 46:251–273. doi:10.1016/0306-4522(92)90049-8, PMID: 1311812
11. Houston CM, Hosie AM, Smart TG (2008) Distinct regulation of β2 and β3 subunit-containing cerebellar synaptic $GABA_A$ receptors by calcium/calmodulin-dependent protein kinase II. J Neurosci 28:7574–7584. doi:10.1523/JNEUROSCI.5531-07.2008, PMID: 18650335
12. Houston CM, He Q, Smart TG (2009) CaMKII phosphorylation of the $GABA_A$ receptor: receptor subtype- and synapse-specific modulation. J Physiol 587:2115–2125. doi:10.1113/jphysiol.2009.171603, PMID: 19332484
13. Huang RQ, Dillon GH (1998) Maintenance of recombinant type A γ-aminobutyric acid receptor function: role of protein tyrosine phosphorylation and calcineurin. J Pharmacol Exp Ther 286:243–255, PMID: 9655866
14. Imanishi T, Yamanaka H, Rhee JS, Akaike N (1996) Interaction between the intracellular Ca^{2+} stores in rat dissociated hippocampal neurones. Neuroreport 7:1421–1426, PMID: 8856690

15. Inoue M, Oomura Y, Yakushiji T, Akaike N (1986) Intracellular calcium ions decrease the affinity of the GABA receptor. Nature 324:156–158. doi:10.1038/324156a0, PMID: 2431316
16. Inoue M, Akaike N (1988) Blockade of γ-aminobutyric acid-gated chloride current in frog sensory neurons by picrotoxin. Neurosci Res 5:380–394. doi:10.1016/0168-0102(88)90024-7, PMID: 2456501
17. Irving AJ, Collingridge GL, Schofield JG (1992) Interactions between Ca^{2+} mobilizing mechanisms in cultured rat cerebellar granule cells. J Physiol 456:667–680, PMID: 1338107
18. Jones MV, Westbrook GL (1995) Desensitized states prolong $GABA_A$ channel responses to brief agonist pulses. Neuron 15:181–191. doi:10.1016/0896-6273(95)90075-6, PMID: 7542462
19. Jones MV, Westbrook GL (1997) Shaping of IPSCs by endogenous calcineurin activity. J Neurosci 17:7626–7633, PMID: 9315884
20. Jones MV, Sahara Y, Dzubay JA, Westbrook GL (1998) Defining affinity with the $GABA_A$ receptor. J Neurosci 18:8590–8604, PMID: 9786967
21. Kanematsu T, Takeya H, Watanabe Y, Ozaki S, Yoshida M, Koga T, Iwanaga S, Hirata M (1992) Putative inositol 1,4,5-trisphosphate binding proteins in rat brain cytosol. J Biol Chem 267:6518–6525, PMID: 1313009
22. Kanematsu T, Misumi Y, Watanabe Y, Ozaki S, Koga T, Iwanaga S, Ikehara Y, Hirata M (1996) A new inositol 1,4,5-trisphosphate binding protein similar to phospholipase C-δ1. Biochem J 313:319–325, PMID: 8546702
23. Kanematsu T, Jang IS, Yamaguchi T, Nagahama H, Yoshimura K, Hidaka K, Matsuda M, Takeuchi H, Misumi Y, Nakayama K, Yamamoto T, Akaike N, Hirata M, Nakayama K (2002) Role of the PLC-related, catalytically inactive protein p130 in $GABA_A$ receptor function. EMBO J 21:1004–1011. doi:10.1093/emboj/21.5.1004, PMID: 11867528
24. Khodakhah K, Armstrong CM (1997) Inositol trisphosphate and ryanodine receptors share a common functional Ca^{2+} pool in cerebellar Purkinje neurons. Biophys J 73:3349–3357. doi:10.1016/S0006-3495(97)78359-0, PMID: 9414245
25. Kincaid RL, Balaban CD, Billingsley ML (1987) Differential localization of calmodulin-dependent enzymes in rat brain: evidence for selective expression of cyclic nucleotide phosphodiesterase in specific neurons. Proc Natl Acad Sci U S A 84:1118–1122, PMID: 3029762
26. Kuno T, Mukai H, Ito A, Chang CD, Kishima K, Saito N, Tanaka C (1992) Distinct cellular expression of calcineurin Aα and Aβ in rat brain. J Neurochem 58:1643–1651. doi:10.1111/j.1471-4159.1992.tb10036.x, PMID: 1313851
27. Lalo UV, Kostyk PG (1998) Depletion of caffeine-sensitive calcium store results in diminution of ATP-induced metabotropic calcium responses in rat neocortical neurons. Neurophysiology 30:289–292. doi:10.1007/BF02462840
28. Martina M, Mozrzymas JW, Boddeke HW, Cherubini E (1996) The calcineurin inhibitor cyclosporin A-cyclophilin A complex reduces desensitization of $GABA_A$-mediated responses in acutely dissociated rat hippocampal neurons. Neurosci Lett 215:95–98. doi:10.1016/0304-3940(96)12957-8, PMID: 8888004
29. McPherson PS, Kim YK, Valdivia H, Knudson CM, Takekura H, Franzini-Armstrong C, Coronado R, Campbell KP (1991) The brain ryanodine receptor: a caffeine-sensitive calcium release channel. Neuron 7:17–25. doi:10.1016/0896-6273(91)90070-G, PMID: 1648939
30. Mizokami A, Kanematsu T, Ishibashi H, Yamaguchi T, Tanida I, Takenaka K, Nakayama KI, Fukami K, Takenawa T, Kominami E, Moss SJ, Yamamoto T, Nabekura J, Hirata M (2007) Phospholipase C-related inactive protein is involved in trafficking of γ2 subunit-containing $GABA_A$ receptors to the cell surface. J Neurosci 27:1692–1701. doi:10.1523/JNEUROSCI.3155-06.2007, PMID: 17301177
31. Mizokami A, Tanaka H, Ishibashi H, Umebayashi H, Fukami K, Takenawa T, Nakayama KI, Yokoyama T, Nabekura J, Kanematsu T, Hirata M (2010) $GABA_A$ receptor subunit alteration-dependent diazepam insensitivity in the cerebellum of phospholipase C-related inactive protein knockout mice. J Neurochem 114:302–310. doi:10.1111/j.1471-4159.2010.06754.x, PMID: 20412381
32. Mouginot D, Feltz P, Schlichter R (1991) Modulation of GABA-gated chloride currents by intracellular Ca^{2+} in cultured porcine melanotrophs. J Physiol 437:109–132, PMID: 1653849
33. Mozrzymas JW, Cherubini E (1998) Changes in intracellular calcium concentration affect desensitization of $GABA_A$ receptors in acutely dissociated P2–P6 rat hippocampal neurons. J Neurophysiol 79:1321–1328, PMID: 9497413
34. Muller MS, Obel LF, Waagepetersen HS, Schousboe A, Bak LK (2013) Complex actions of ionomycin in cultured cerebellar astrocytes affecting both calcium-induced calcium release and store-operated calcium entry. Neurochem Res 38:1260–1265. doi:10.1007/s11064-013-1021-4, PMID: 23519933
35. Newland CF, Cull-Candy SG (1992) On the mechanism of action of picrotoxin on GABA receptor channels in dissociated sympathetic neurones of the rat. J Physiol 447:191–213, PMID: 1317428
36. Orser BA, Wang LY, Pennefather PS, MacDonald JF (1994) Propofol modulates activation and desensitization of $GABA_A$ receptors in cultured murine hippocampal neurons. J Neurosci 14:7747–7760, PMID: 7996209
37. Ramakrishnan L, Hess GP (2005) Picrotoxin inhibition mechanism of a γ-aminobutyric acid A receptor investigated by a laser-pulse photolysis technique. Biochemistry 44:8523–8532. doi:10.1021/bi0477283, PMID: 15938643
38. Shmigol A, Kostyuk P, Verkhratsky A (1994) Role of caffeine-sensitive Ca^{2+} stores in Ca^{2+} signal termination in adult mouse DRG neurones. Neuroreport 5:2073–2076. doi:10.1007/BF00374686, PMID: 7865748
39. Stelzer A (1992) Intracellular regulation of $GABA_A$-receptor function. Ion Channels 3:83–136, PMID: 1384761
40. Takenaka K, Fukami K, Otsuki M, Nakamura Y, Kataoka Y, Wada M, Tsuji K, Nishikawa S, Yoshida N, Takenawa T (2003) Role of phospholipase C-L2, a novel phospholipase C-like protein that lacks lipase activity, in B-cell receptor signaling. Mol Cell Biol 23:7329–7338. doi:10.1128/MCB.23.20.7329-7338.2003, PMID: 14517301
41. Uji A, Matsuda M, Kukita T, Maeda K, Kanematsu T, Hirata M (2002) Molecules interacting with PRIP-2, a novel $Ins(1,4,5)P_3$ binding protein type 2: comparison with PRIP-1. Life Sci 72:443–453. doi:10.1016/S0024-3205(02)02275-0, PMID: 12467885
42. Vigh J, Lasater EM (2003) Intracellular calcium release resulting from mGluR1 receptor activation modulates $GABA_A$ currents in wide-field retinal amacrine cells: a study with caffeine. Eur J Neurosci 17:2237–2248. doi:10.1046/j.1460-9568.2003.02652.x, PMID: 12814357
43. Vriens J, Appendino G, Nilius B (2009) Pharmacology of vanilloid transient receptor potential cation channels. Mol Pharmacol 75:1262–1279. doi:10.1124/mol.109.055624, PMID: 19297520
44. Wang RA, Cheng G, Kolaj M, Randic M (1995) α-Subunit of calcium/calmodulin-dependent protein kinase II enhances γ-aminobutyric acid and inhibitory synaptic responses of rat neurons in vitro. J Neurophysiol 73:2099–2106, PMID: 7623101